2023

Evolution and Environmental Controls of Area Updraft Proxies in QLCSs Observed in PERiLS-2022

Celia Werner
celia.werner@stonybrook.edu

Evolution and Environmental Controls of Area Updraft Proxies in QLCSs Observed in PERiLS-2022

A Thesis presented

by

Celia Grace Werner

to

The Graduate School

in Partial Fulfillment of the

Requirements

for the Degree of

Master of Science

in

Atmospheric and Oceanic Sciences

Stony Brook University

October 2023

Stony Brook University
The Graduate School

Celia Grace Werner

We, the thesis committee for the above candidate for the
Master of Science degree, hereby recommend
acceptance of this thesis.

Michael M. French – Thesis Advisor
Associate Professor, School of Marine and Atmospheric Sciences, Stony Brook University

---

Brian A. Colle
Professor, School of Marine and Atmospheric Sciences, Stony Brook University

---

Kristin M. Calhoun
Research Scientist, National Severe Storms Laboratory

This thesis is accepted by the Graduate School

Celia Marshik
Dean of the Graduate School

Abstract of the Thesis

Evolution and Environmental Controls of Area Updraft Proxies in QLCSs Observed in PERiLS-2022

by

Celia Grace Werner

Master of Science

in

Atmospheric and Oceanic Sciences

Stony Brook University

2023

Results from recent modeling and observational work have connected the size or area of convective updrafts with hazardous weather, including tornadoes and large hail. Additional studies have hypothesized that elements of the near-storm environment (NSE) controls updraft size. However, observationally, little is known about the evolution of updraft sizes in quasi-linear convective systems (QLCSs) and what impact the NSE has on the updraft sizes at mid-levels. A recent and ongoing multi-agency integrated field project focused on better understanding the development and life cycles of tornadoes in QLCSs provides an opportunity to do so. The Propagation, Evolution, and Rotation in Linear Storms (PERiLS) field project completed its first year of deployments in March-May of 2022 in the Southeast U.S. In 2022, there were four PERiLS Intensive Observation Periods (IOPs), each lasting several hours.

WSR-88D and extensive near storm environment data were analyzed in a detailed study of the relationship between the changes in midlevel updraft size proxies (Z_{DR} columns) and any

changes in the NSE. In order to mimic information that would be available to forecasters, data from the nearby WSR-88D radars were used to estimate QLCS updraft size and variability over time using Z_{DR} column size as an updraft size proxy. These data were then combined with NSE data obtained by the multitude of mobile sounding teams on PERiLS. The main topics of study include: single and total updraft size variability throughout deployment periods and spatial and temporal changes in the NSE that are evident as observable changes in updraft proxy size. All four deployments had at least one substantial individual updraft growth throughout the duration of the QLCS. Three out of the four PERiLS IOPs provided usable NSE data around the time of these updraft growths. Contrary to previous findings in supercell studies, the LCL heights and the storm-relative winds decreased during the time of an updraft growth. In times when updrafts did not change in size, LCL heights and storm-relative winds either increased or stayed the same. Reasoning behind the null result and future avenues for research are also discussed.

Table of Contents

List of Figures

List of Tables

List of Abbreviations

MCS: Mesoscale Convective System

QLCS: Quasi-linear convective system

OT: overshooting top

OTA: overshooting top area

Z_{DR}: differential reflectivity

SR: storm-relative

SRH: storm-relative helicity

MCV: mesoscale convective vortex

NSE: near-storm environment

PERiLS: Propagation, Evolution, and Rotation in Linear Storms

IOPs: Intensive Observation Periods

WDSS-II: Weather Decision Support System - Integrated Information

TRENDSS: Thunderstorm Risk Estimation and Nowcasting Development from Size Sorting

Acknowledgments

I would first like to thank my advisor Dr. Michael French for all his continual support, understanding, guidance, and mentorship these past two years. The wisdom he shared, the example he set, and the experiences he made possible through field projects and conferences are memories and knowledge I will take with me throughout my lifetime. My time at Stony Brook will always be treasured most impart to his compassion and advisement. I appreciate funding from NOAA grant NA21OAR4320204 in order to perform this research.

I would like to thank the rest of my committee, Dr. Brian Colle and Dr. Kristen Calhoun for their insight and expertise as well. Their suggestions and willingness to help promote research for young scientists has made this process so much more educational and enriching.

Finally, I would like to thank all of my family, friends, classmates, and other faculty members who helped me get to this point. Their continual love and support, either academically or personally, has been invaluable in my collegiate career. Thank you.

1 Introduction

1.1 Background and Motivation

The unpredictable nature of hazardous weather, including straight-line winds, flash floods, hail, lightning, and tornadoes associated with deep moist convection require accurate and timely forecasts and warnings to best serve the public. Of the various modes of convection, supercell thunderstorms are known to have the most destructive impacts (e.g., Smith et al. 2012). However, increasingly research is focused on mesoscale convective systems (MCSs), or more specifically quasi-linear convective systems (QLCSs). MCSs are roughly defined by being at least 100 km in spatial scale and lasting for at least 3 hours. QLCSs are a specific type of MCS in which the storms are oriented along a long and narrow axis (e.g., Schumacher and Rasmussen 2020). Just as for any deep moist convection, QLCS organization and intensification require sufficient moisture, instability, and lift and also involve vertical wind shear and cold pool interactions that determine, in part, the system's evolution.

Despite a research focus on supercell thunderstorms, severe/straight-line winds, flash floods, hail, lightning, and tornadoes associated with QLCSs can be costly, destructive, and deadly. For example, MCSs produce more than half of the yearly accumulated rainfall in many areas of the U.S. (e.g., Haberlie and Ashley 2018). In addition, though QLCS tornadoes tend to be weaker than those from supercells, nearly a quarter of all tornadoes in the U.S. come from QLCSs (Smith et al. 2012) and they disproportionately occur at night (Trapp et al. 2005). QLCS tornadoes also tend to have short warning lead times (Brotzge et al. 2013), and so combined with their nocturnal tendencies, their occurrence can be more deadly than those that occur during the day (e.g., Ashley et al. 2008). With advancements made in convection allowing models, available operationally since the late 2000s, representation of MCS development and evolution has improved (Kain et al.

2008; Schwartz et al. 2009). However, QLCS tornadoes remain difficult to forecast, particularly in marginally-severe storm environments. As a result, any ability to identify features and characteristics in real-time that may provide information about the impending evolution of a QLCS are likely to be valuable to researchers and forecasters alike.

One such feature has been the subject of recent theoretical, modeling, and observational research is the area of the midlevel and low-level storm updraft. It is self-evident that the updraft is a key component of any convective system, and its characteristics may be important for the system's evolution. Recent work(Trapp et al. 2017; Marion et al. 2019; Sessa and Trapp 2020; Marion and Trapp 2021; French and Kingfield 2021) has directly and perhaps surprisingly linked the *size* of convective updrafts with tornado intensity, including before tornadoes even form, possibly introducing a new tool to incorporate into forecasting and nowcasting (i.e., 0-1 hour forecasting) tornado intensity. This link has been made in both supercells and QLCSs but may be more direct in supercells. However, what is not as well understood, and is one of the motivating objectives of this work, is *why* updraft size has shown to be strongly associated with tornado intensity.

Trapp et al. (2017) argued, using theory, and supported by model simulations, that wider updrafts should lead to both wider and stronger tornadoes based on the conservation of angular momentum arguments and Kelvin's circulation theorem. They found strong linear correlations between updraft area and midlevel and near-ground cyclone area, near-ground vertical velocity, and tornado scale in idealized simulations, which provided initial evidence that updraft area may be used as a predictive tool for tornado intensity (e.g., Fig. 1a). Coffer and Markowski (2018) provided some skepticism to this idea, arguing through a set of higher resolution simulations that there is not a strong relationship between updraft size and tornado intensity. Trapp et al. (2018)

disagreed, saying the Coffer and Markowski (2018) simulations used only a narrow set of environmental parameters and reaffirmed their findings using higher resolution simulations.

A difficult problem in attempting to verify Trapp et al. (2017) ideas using observations is how to estimate updrafts size using conventional observations. Trapp et al. (2017) suggested that one possibility is to use the area of the overshooting top (OT; e.g., Bedka et al. 2010) in satellite data as a proxy for updraft area. Building off of Trapp et al. (2017), Marion et al. (2019) explored the use of overshooting top area (OTA), using brightness cloud top temperatures from satellite data, as a proxy for updraft area and to compare with tornado intensity. A strong updraft would create higher cloud tops, extending them into the stratosphere, as compared to the cloud cover within the rest of the storm. Therefore, storms with larger updrafts would likely see a larger OT and bigger OTA. Using a sample of 30 storms, they found there was indeed a strong positive relationship between OTA and tornado EF-scale rating (Fig. 1b). Larger OTAs were more typically found in supercell cases and smaller areas in QLCS cases, consistent with weaker EF-ratings more often found in QLCSs. Also, given that OTs occur near the top of the troposphere into the stratosphere, the OTA used is best thought of as a mid- to upper-level (3-6+km) updraft proxy rather than a low-level (1-3 km) updraft proxy.

Subsequent observational work in Sessa and Trapp (2020) estimated updraft size by measuring the width of low-level mesocyclones in a larger sample of 102 storms using radial velocity data. They also found a strong relationship between supercell mesocyclone width and EF rating (Fig. 1c), but again the signal was weaker in QLCSs than in supercells. This is most likely due to the more shallow and transient nature of most QLCS mesocyclones.

French and Kingfield (2021) identified another way to estimate updraft size: the area of the differential reflectivity (Z_{DR}) column in real-time radar data. The Z_{DR} column is defined as a

typically narrow (4-8 km wide) vertical extension of positive Z_{DR} values above the 0˚C level (e.g., Kumjian et al. 2014). This radar signature is representative of large water droplets, which have a larger Z_{DR} (> 1 dB) than dry snow (~0 dB), being lofted above the environmental freezing level due to a strong updraft. The Z_{DR} column is generally co-located with the updraft and the weak echo region in radar reflectivity. The Z_{DR} column can be used as a predictive tool for hail as the peak column area precedes surface hail signatures (Picca et al. 2010; Kumjian et al 2014). Recent studies have found a more general relationship with hazardous weather; for example, Kuster et al. (2019) found that severe storms had wider and deeper Z_{DR} columns as compared to non-severe storms.

French and Kingfield (2021) then modified an algorithm developed by Kingfield and Picca (2018; see details in section 2) to partially automate the calculation of Z_{DR} column areas. They compared a large sample (198) of tornadic and nontornadic supercells and also examined supercells producing tornadoes of different intensities. Consistent with previous studies, a strong positive correlation was found between larger Z_{DR} column areas *before a tornado formed* and tornado intensity, with a clear distinction between EF3+ tornados and weaker tornadoes. Z_{DR} columns were also found to be larger in tornadic supercells in the radar scans immediately before tornadogenesis as compared to nontornadic supercells immediately before the maximum low-level shear, even when only weakly tornadic supercells were compared (Fig. 2). The latter result is consistent with Van Den Broeke (2020), who found, using a smaller sample size of 63 supercells, that Z_{DR} columns in tornadic supercells are larger and less variable than in nontornadic supercells 30 minutes prior to tornadogenesis. French and Kingfield (2021) did not examine QLCSs in their sample, but their results introduce the possibility of a skillful tornadogenesis component to updraft area as well.

A number of studies, from theory, modeling, and observations conclude independently that there is a relationship between updraft size and tornado intensity, providing strong evidence that there is a link between the two. However, less clear is *why*: what is the mechanism for this relationship? An emerging amount of research provides an alternative to the Trapp et al. (2017) hypothesis. The alternative can be summarized as what we call the *shared environmental pathways hypothesis*. This idea can be explained as: the connection between updraft size and tornado intensity is indirect and results from both tornado intensity and large updrafts being driven by similar environmental conditions.

Results from Trapp et al. (2017) imply that the 0-2 km hodograph radius was correlated with updraft radius. In an unrelated study, Warren et al. (2017) found that one of the important drivers for updraft area is upper-level vertical wind shear, which increases low-level storm-relative flow. Simulations from Peters et al. (2019) verified the Warren et al. (2017) results and found that as storm-relative low-level flow increases, there is greater mass flux into updrafts, and the greater storm-relative flow occurs when deep-layer shear is stronger. Given the known importance of storm-relative helicity (SRH) to tornadoes (e.g., Coffer et al. 2019), one idea is that environments with large SRH (a product of storm-relative winds and streamwise vorticity) lead to both large updrafts and stronger tornadoes. Follow-up work by Peters et al. (2020) clarified the relationship between SRH and updraft size (Fig. 3). They found that SRH and streamwise vorticity were *not* correlated to updraft width (Fig. 3a,b), but that storm-relative winds and deep-layer shear were correlated with updraft width (Fig. 3c,d). LCLs are also likely to factor into updraft size. Mulholland et al. (2021) simulated storms within horizontally homogeneous idealized environments using three different depths of a dry adiabatic lapse rate layer to produce the differing LCL heights. It was found that storms that formed in the higher LCL environments tended to have

the largest horizontal maximum buoyancy, vertical velocity, and larger updrafts, though the direct relationship was not always clear in their simulations.

Only recently have studies focused specifically on updraft size in QLCSs. Marion and Trapp (2021) designed a modeling study to determine the controls of QLCS tornado intensity and hypothesized that one reason QLCS tornadoes may be weaker is that the low-level updrafts are smaller. Consistent with this hypothesis, they found that low-level mesoscale convective vortex (MCV) width within a QLCS is one of the main controls on tornado intensity within these systems. This finding for QLCSs is consistent with the reasonings of Trapp et al. (2017), even though that theoretical framework is based on supercells. The MCV within a QLCS, however, also has differences from low-level mesocyclones; the former tends to not be as deep and persistent as the latter, which they hypothesize may explain why the relationship between updraft size and tornado intensity is weaker in QLCSs than in supercells. They also found that an upright updraft is also important to tornado formation but not necessarily tornado strength; updraft tilt had negligible impact in tornado intensity in their simulations.

Marion and Trapp (2021) also analyzed potential environmental impacts on QLCS tornado intensity. They found that hodograph curvature and strong 0-1 km bulk shear and SRH were tied to stronger tornado-like vortices in their simulations. In their simulations, the cases with a curved hodograph (stronger low-level wind shear) also resulted in a stronger updraft locally due to stronger vertical mixing that led to shallower and weaker cold pools. Simulated straight-line hodograph cases had stronger and larger cold pools but not necessarily stronger tornadoes. Cold pool development and forcings in QLCSs are found to play a major role in the difference between the deep updrafts of supercells and the low-level updrafts in QLCSs. The Marion and Trapp (2021) results again introduce the possibility that low-level shear and SRH may simultaneously influence

updraft size and tornado production and intensity. Other internal processes of the QLCS have also been linked to mesovortex/tornado formation and intensification, such as the release of horizontal shear instability in an initial observational analysis in Carbone (1982, 1983) and the tilting of environmental horizontal vorticity and stretching of leading-edge mesovortices in cool-season QLCSs (Wheatly and Trapp 2008).

Modeling studies also show how the storm environment can affect polarimetric radar signatures. Snyder et al. (2017) used a numerical model to simulate convective systems to study X-band polarimetric radar variables and how they vary in different storm environments. Z_{DR} columns were considerably larger in strong shear cases and were more cylindrically shaped in curved hodograph cases. These simulations also showed a slight displacement of the Z_{DR} column to the west of the maximum vertical velocity within the updraft. The strengthening of these Z_{DR} columns within convective systems indicates a strengthening updraft and can be used to diagnose an intensifying storm. The known controls on QLCS tornado intensity, such as low-level shear mentioned above, and the model simulated controls, wind shear along with hodograph curvature, on the Z_{DR} column can be used as a starting point for studying the observed NSE.

Observationally, little is known about the evolution of updraft sizes in QLCSs and what impact the NSE has on the updraft sizes at both low and midlevels. A recent and ongoing multi-agency integrated field project focused on better understanding the development and life cycles of tornadoes in QLCSs provides an opportunity to do so. The Propagation, Evolution, and Rotation in Linear Storms (PERiLS) field project, designed to improve knowledge and prediction of tornadoes within QLCSs and solely focused on convection in the southeast U.S., completed its first year of deployments in March-May of 2022. In 2022, there were four PERiLS Intensive Observation Periods (IOPs), each lasting several hours. Analysis of WSR-88D, mobile radar, and

NSE data will allow for a detailed study of the relationship, if one exists, between the midlevel updraft size proxies (Z_{DR} columns) and the NSE.

1.2 Objectives

The main objective of this study is to observationally determine the evolution of midlevel area proxies in PERiLS 2022 data and determine if there are NSE controls on updraft area consistent with what previous studies have shown for supercells. WSR-88D data from each IOP are used to calculate the Z_{DR} column areas using a previously developed novel algorithm and data collected from various radiosonde teams will be used to diagnose NSE.

The questions to be addressed in this study are: i) Do LCLs and/or low-level storm-relative winds drive midlevel updraft size? ii) Does QLCS updraft size vary considerably during PERiLS observable time scales (typically between 4-5 hours)? If so, are there corresponding near-storm environment changes? iii) How do updraft sizes vary within a QLCS at one time with any correlation to near-storm environmental changes along the QLCS?

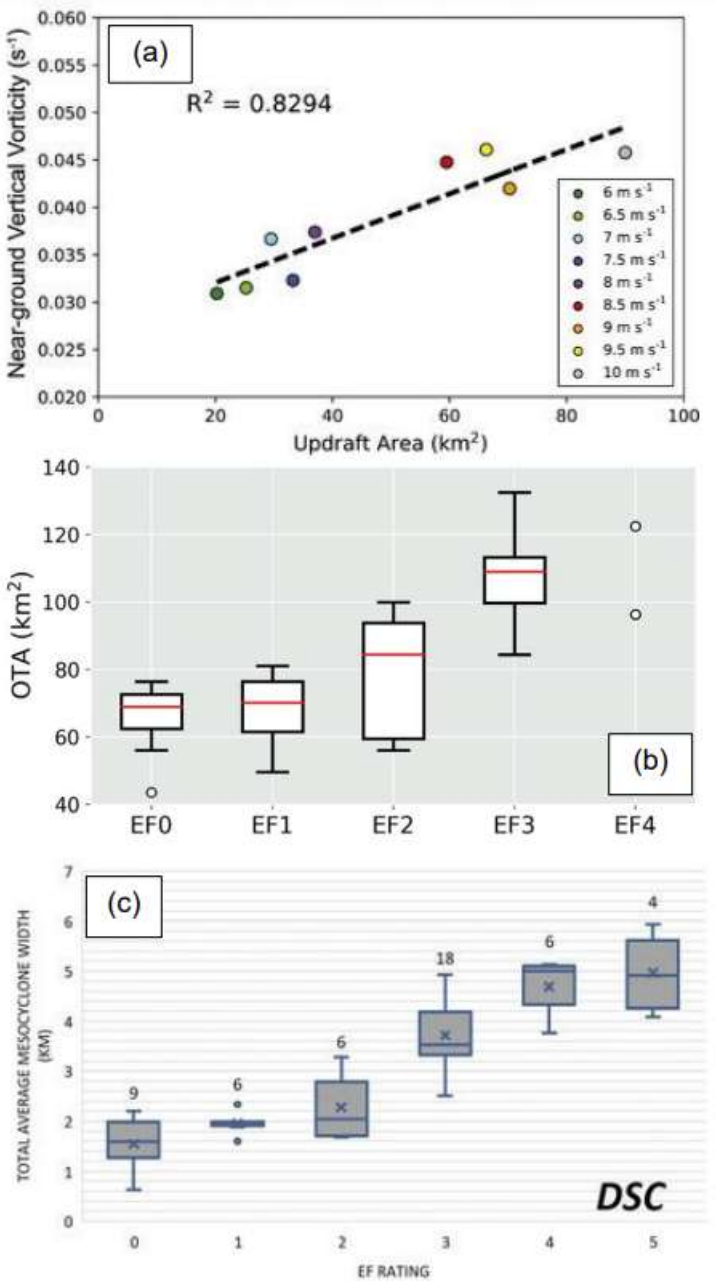

Fig. 1: (a) Scatterplot showing relationship between supercell midlevel (z = 6.25 km) updraft area (km^2) and near-ground vertical vorticity (s^{-1}) from CM1 experiments over a range of hodograph radii (m s^{-1}). Adapted from Trapp et al. (2017). (b) Box and whisker plot of observed overshooting top area (OTA; km2) versus tornado EF scale rating for 30 tornadic supercells. Adapted from Marion et al. (2019). (c) Box-and-whisker plot showing the relationship between the total average pretornadic mesocyclone width (km) EF rating of the resultant tornado for 49 discrete supercells. The mean is represented by the × and the median by the bar. The top and bottom of the box represent the third and first quartiles with exclusive medians, respectively, and the top and bottom whiskers represent the minimum and maximum values, respectively. Adapted from Sessa and Trapp (2020).

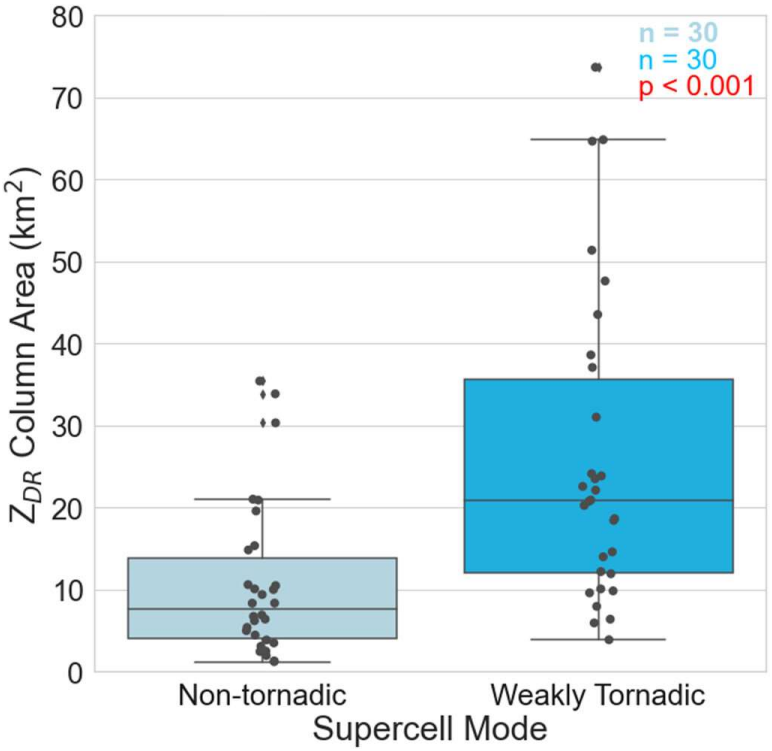

Fig. 2: Box and whisker plot comparing ZDR column areas of nontornadioc cases and the 30 tornadic cases with the weakest ΔV in the tornadic vortex signature associated with the tornado. The box encloses the 25th-75th percentiles, the thin black line marks the median, and the whiskers encompass the rest of the values unless they are more than 1.5 times removed from the interquartile range, in which case they are plotted as outliers. Color-coded sample sizes and the p value for rejecting the hypothesis that both sets of data derive from the same underlying population appear in the top right corner. Adapted from French and Kingfield (2021).

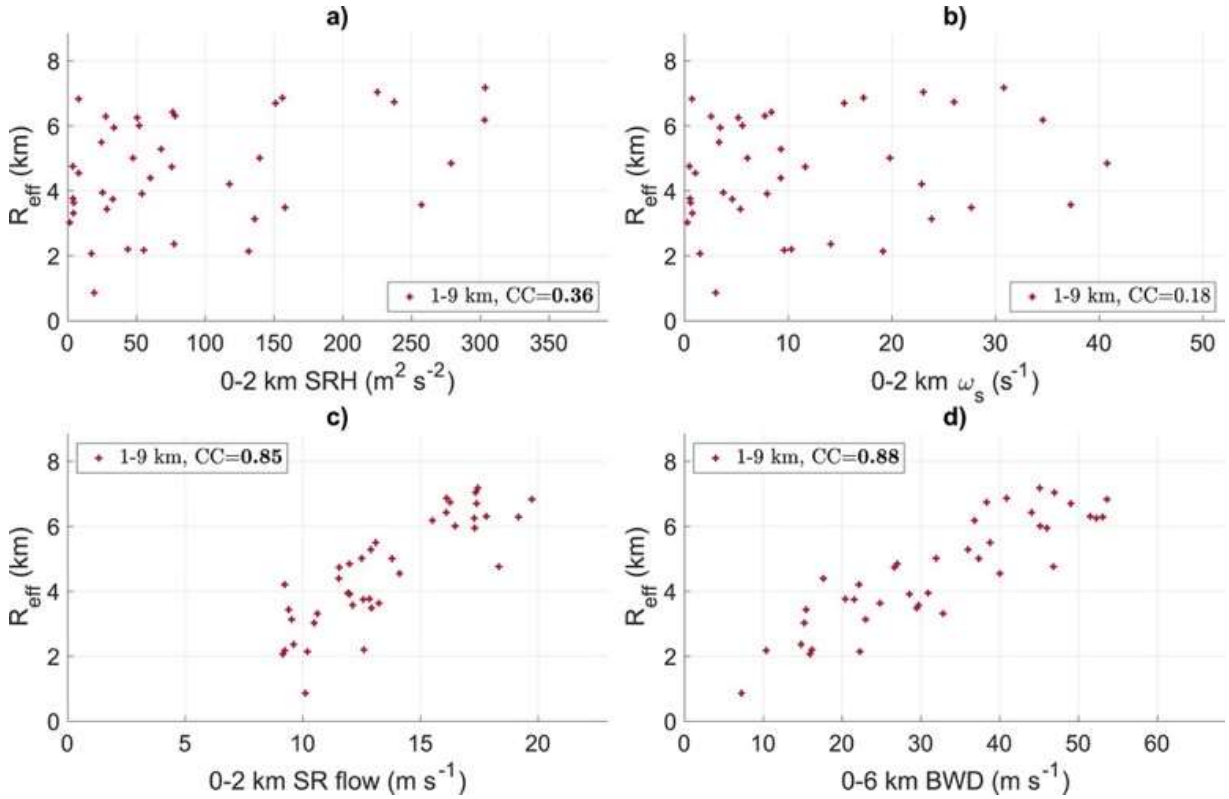

Fig. 3: Scatterplots of 1-3 hour averages of 40 simulated updraft effective radius (km) as a function of (a) 0-2 km SRH (m^2 s^{-2}), (b) 0-2 km streamwise vorticity (s^{-1}), (c) 0-2 km storm-relative flow (m s^{-1}) and (d) 0-6 km bulk wind difference. From Peters et al.

2 Data and Methodology

In 2022, there were four PERiLS IOPs (Table 1) within the PERiLS domain (Fig. 4). In all four cases, QLCSs did form and traverse the PERiLS domain, containing traditional convective lines with trailing stratiform regions of precipitation. However, three of the four IOPs also contained significant precipitation forward of the main convective line, which meant that the conditions sampled by soundings launched in this pre-convective precipitation were not a true indication of the air being ingested by the storm. All four IOPs are examined to determine proxies for midlevel updraft size, near-QLCS environments, and hazardous weather reports. PERiLS instrumentation included several mobile radars, sounding and profiling systems, mobile mesonets, disdrometers, and a lightning mapping array (Fig. 5).[1] PERiLS operated in a "static" (i.e., Eulerian) domain configuration where most instrumentation stayed in one location while the QLCS moved through, given the number of assets and the expected rapid propagation speed of the QLCSs. The PERiLS static domain is counter to past severe storm projects, for example VORTEX-2, that attempted to move with storms (i.e., Lagrangian). The PERiLS domain necessitated accurate forecasting of QLCS intensity and location 2-3 days out in order for teams to properly plan. Inevitably, some IOPs had a mismatch between asset locations, including those used in this study, and ideal placement relative to the QLCS.

2.1 Z_{DR} Column Area

To estimate midlevel updraft size, Z_{DR} column *area* is calculated instead of *width*, as done in previous studies, to account for the irregular shapes of Z_{DR} columns (in many cases, width would

[1] A complete listing of the teams involved in PERiLS can be found at: https://www.nssl.noaa.gov/projects/perils/.

not be an accurate representation of the size of the updraft). The updraft areas are estimated using Z_{DR} column areas from an algorithm developed for use in the Weather Decision Support System - Integrated Information (WDSS-II; French and Kingfield 2021) using WSR-88D data. The origin of this algorithm is Kingfield and Picca (2018), who developed the Thunderstorm Risk Estimation and Nowcasting Development from Size Sorting (TRENDSS) algorithm. TRENDSS was used to identify both Z_{DR} columns and another polarimetric radar signature, the low-level Z_{DR} arc. For French and Kingfield (2021), the authors modified TRENDSS as described below so that it only identifies Z_{DR} columns (e.g., Fig. 6).

The Z_{DR} column is isolated as an object of contiguous Z_{DR} that is at least two standard deviations above the mean Z_{DR} for that radar scan closest to 1 km above the 0˚C level (estimated from the 13-km RAP). The standard deviation approach used has a significant advantage over traditional algorithms that identify Z_{DR} columns using a 1.0 or 1.5 dB Z_{DR} cutoff (e.g., Snyder et al. 2015) in its immunity to Z_{DR} bias, which can be high (e.g., Tuftedal et al. 2021). As a result, no Z_{DR} bias correction is used in this study. Further, to ensure meteorological targets are sampled, for each elevation angle of radar data, a Z_{DR} bin must also have a $\rho_{HV} > 0.8$, mitigating non-meteorological scatterers and $Z_{DR} < 6$ dB, mitigating biological scatterers. The quality-controlled output results in a field of Z_{DR} anomalies for each bin. Given that away from the Z_{DR} column above the 0˚C level, dry snow aggregates dominate with Z_{DR} near 0 dB, the Z_{DR} column typically contains values that are at least two standard deviations above the mean. Since Z_{DR} columns rarely extend more than a few km above the 0˚C level, 1 km is high enough to provide confidence that a defined Z_{DR} area is located above the 0˚C level, but low enough so as to not exclude the height of shallower updrafts typically seen within QLCSs compared to supercells.

To simplify analysis given the large number of scans analyzed for this study, the algorithm was enhanced so that it automatically provided the elevation angle closest to 1 km above the 0˚C level (bottom center panels in Fig. 6). Z_{DR} column areas were sensitive to the elevation angle chosen. In order to best capture shallow updrafts without contaminating the Z_{DR} data with liquid water below the 0˚C level, a +/- 750m threshold was established to determine which angle should be chosen to calculate the areas. If the algorithm identified, for example, 0.9˚ elevation angle as that closest to 1 km above the 0˚C level, but at the 0.5˚ elevation, there was a much more significant area, the larger area at 0.5˚ elevation was recorded as long as the height of the beam was within 750 m threshold. If not met, the suggested elevation, even if areas were near 0 km^2, were taken. An example of how the algorithm works is shown for two times during IOP1, prior to (Fig. 6a) and after (Fig. 6b) a significant increase in QLCS updraft area.

As discussed in French and Kingfield (2021), even with these standardization calculations in place, there are still times in which the column areas cannot be unambiguously identified. The most common reason for lack of a column area is interference of a (typically) large Z_{DR} column with the melting layer, which also displays enhanced Z_{DR} values. If the two features could not be easily distinguished, then the areas were not included in the analyses. Also, the use of a static domain in PERiLS means that QLCSs passed right over the WSR-88D system, so at some times, even at the highest elevation angle, a Z_{DR} column could not be identified until the QLCS passed to the east of the radar.

To identify regions of interest, many locations along the leading edge of the QLCS in each IOP were chosen to determine potential updrafts / Z_{DR} columns once the QLCS entered the PERiLS radar domain. When a Z_{DR} column area was identified at the provided elevation angle, the corresponding areas were recorded, and that feature was tracked throughout the lifetime of the

QLCS in the domain. If there were column areas directly adjacent to one another that the algorithm identified as separate features, those areas were added together and recorded as one updraft signature, again consistent with French and Kingfield (2021). Also, in cases where there was no area present at the provided elevation angle, or if it was on the border of two elevation angles, the larger area was taken at the next lowest angle. The total updraft proxy area was also calculated by adding all individual Z_{DR} column areas present at one time to estimate the total size of QLCS updrafts throughout the lifetime of the QLCS within the domain.

2.2 Near-storm Environmental Data

The NSE data used in this study are from ~20 individual radiosonde teams, located at several locations within the domain (typically spaced < 10 km apart) and launched frequently throughout the IOPs (Fig. 7). The main two variables of interest, based on the past work summarized in section 1, are LCL heights (Mulholland et al. 2021) and storm-relative winds (Peters et al. 2020). For all four IOPs, to analyze these two variables, the Sounding/Hodograph Analysis and Research Program in Python (SHARPpy) was used to produce skew-T charts for LCL heights and table sounding data was used to identify total wind speeds at the lowest level closest to the ground and at 500 m. Time periods were then identified in each IOP when there was a significant Z_{DR} column area growth. Unfortunately, IOP3 did not have any usable sounding data by the time the QLCS had formed into a discernable line. Virtually every IOP3 sounding was launched in precipitation (Fig. 7c), preventing accurate sampling of the NSE for the purposes of this study. Each team individually quality controlled their sounding data. Common issues were soundings that prematurely terminated, and issues with accuracy on individual sensors on some launches. All data used in this study were deemed acceptable for use by the PERiLS teams that

obtained the data and uploaded their data to the UCAR Earth Observing Laboratory's PERiLS data management archive service. In working with radiosonde data, we did not encounter obvious indications of problematic data, but such errors cannot be ruled out.

Using NSE data from IOPs 1, 2, and 4, the storm-relative winds were calculated by first finding the u- and v-components of the wind from the total winds at the surface and then at 500 m. Then, the storm motion (magnitude and direction) was estimated by taking the leading edge of the line in radar reflectivity and recording the x and y coordinates of three different parts of that line every 30-minutes centered on the time period that the significant changes in the updraft area occurred (e.g., left panels in Fig. 6). The change in distance, speed, and direction of these three parts of the line were calculated and then averaged to get the storm motion for the 30-minute time frame. An average was done to take into account that different parts of the QLCS move at different speeds and directions as well as to mitigate the inherent subjectivity in using reflectivity (or any radar variable) of the leading edge of the line to estimate QLCS motion. The storm motion, broken down into u- and v-components as well, was then subtracted from the wind components at the surface and the 500 m level at each relevant sounding location to estimate the storm-relative winds at that location of the QLCS closest to the sounding in question. Despite the averaging, we cannot rule out that subjective tracking of parts of the line contribute to uncertainty in the line motion and, therefore uncertainty in the SR wind estimates.

Taking into account the high shear, low CAPE environments more typical for cool season QLCSs in the Southeast U.S., CAPE and wind shear, were calculated as well. The average CAPE value was calculated from each of the sounding teams' data during the IOP times of interest (Table 2) to give an overview of the environment for each storm. The low-level and bulk wind (BWD) from 0-6 km was found by either using the wind at each level and subtracting or it was taken right

from the SHARPpy sounding output. The shear values were then averaged over the same time period. The average CAPE values were on the low side even for cold season QLCSs (300-430 J kg^{-1}) and could indicate some convective contamination from the pre-line rain and convection discussed previously. The 0-6 km wind shear was relatively high and highest for IOP 2; the 0-1 km shear was also consistently large, around 21 m/s for each IOP.

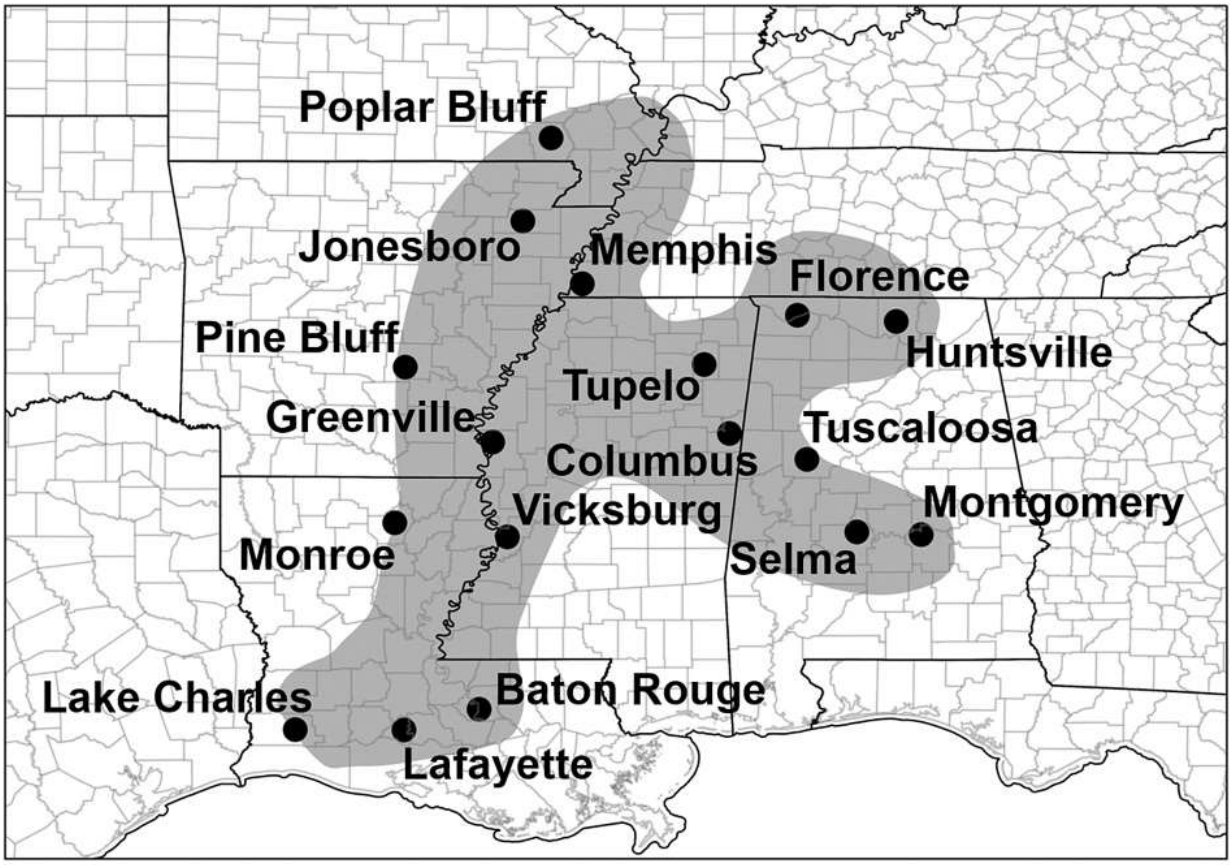

Fig. 4: Approximate operating domain (shaded) of the PERiLS field project in 2022-23. Notable cities also annotated. From PERiLS NOAA Science Plan.

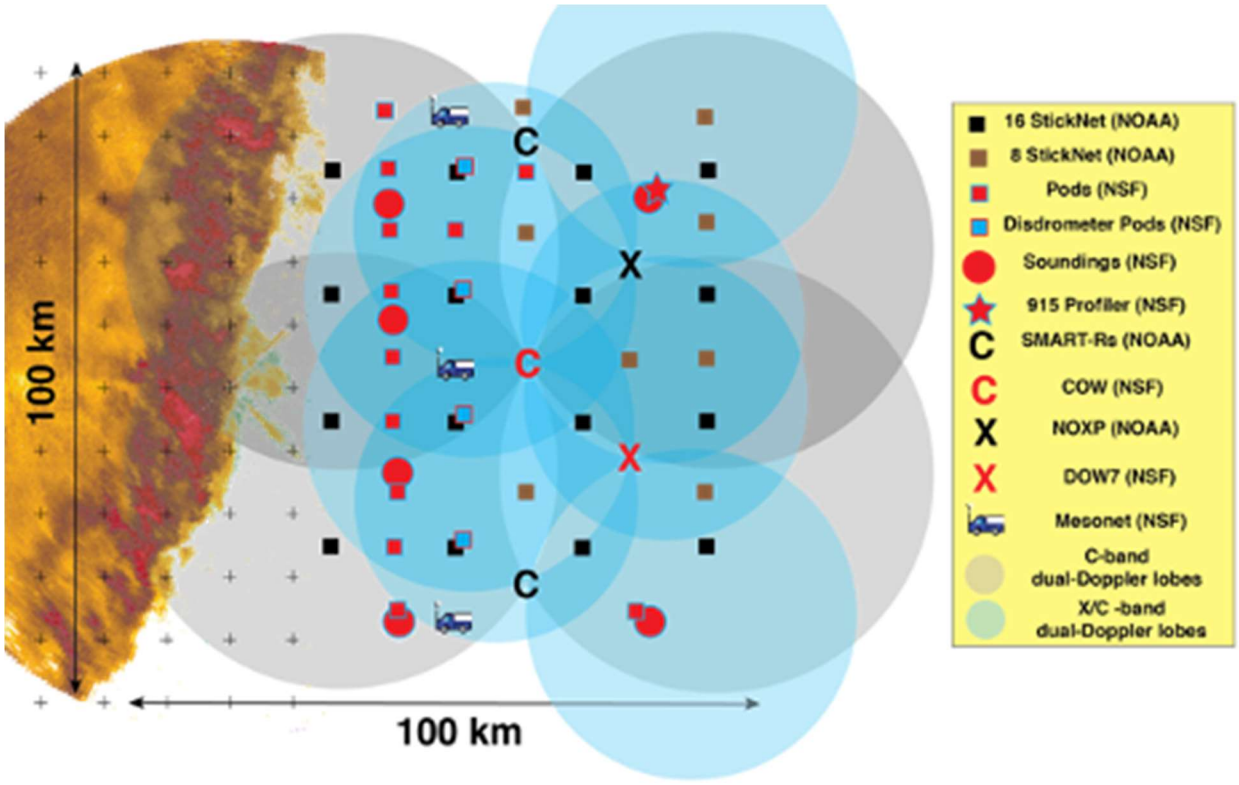

Fig. 5: Idealized deployment strategy for observational assets used for PERiLS in 2022-23, including the locations of mobile radars (letters indicating radar band), Eulerian surface observations (denoted by squares), Lagrangian surface observations (denoted by vehicle icon), and radiosondes (denoted by circles). Idealized dual-Doppler analysis lobes are also denoted as large gray and blue circles. From PERiLS NOAA Science Plan.

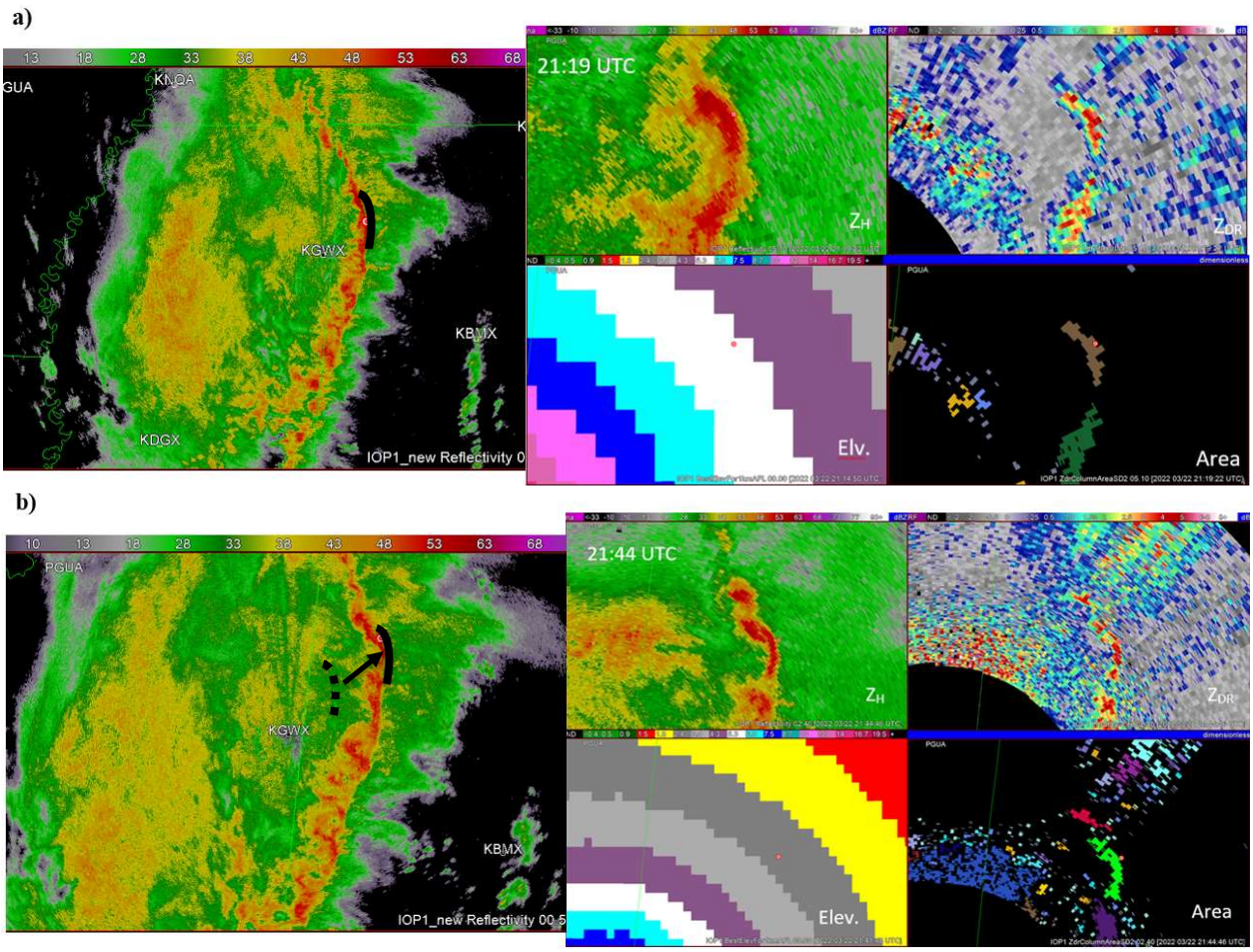

Fig. 6: Four panels depicting how Z_{DR} column area is calculated and evolving in an example from 21:19 to 21:44 UTC in IOP1. (Left) A snapshot of the whole QLCS at 0.5° elevation angle, (top center) reflectivity (Z_H) in dBZ, (top right) differential reflectivity (Z_{DR}) in dB, (bottom center) map depicting which elevation angle is closest to 1 km above 0°C level for the area of interest, indicated by red dot, (bottom right) Z_{DR} column areas for each object. **a)** 21:19 UTC northern updraft calculated at a 5.1° elevation angle **b)** 21:44 UTC northern updraft calculated at 2.4° elevation angle. The black lines and arrow annotated in the top and bottom left panels depict how line motion was estimated using radar reflectivity.

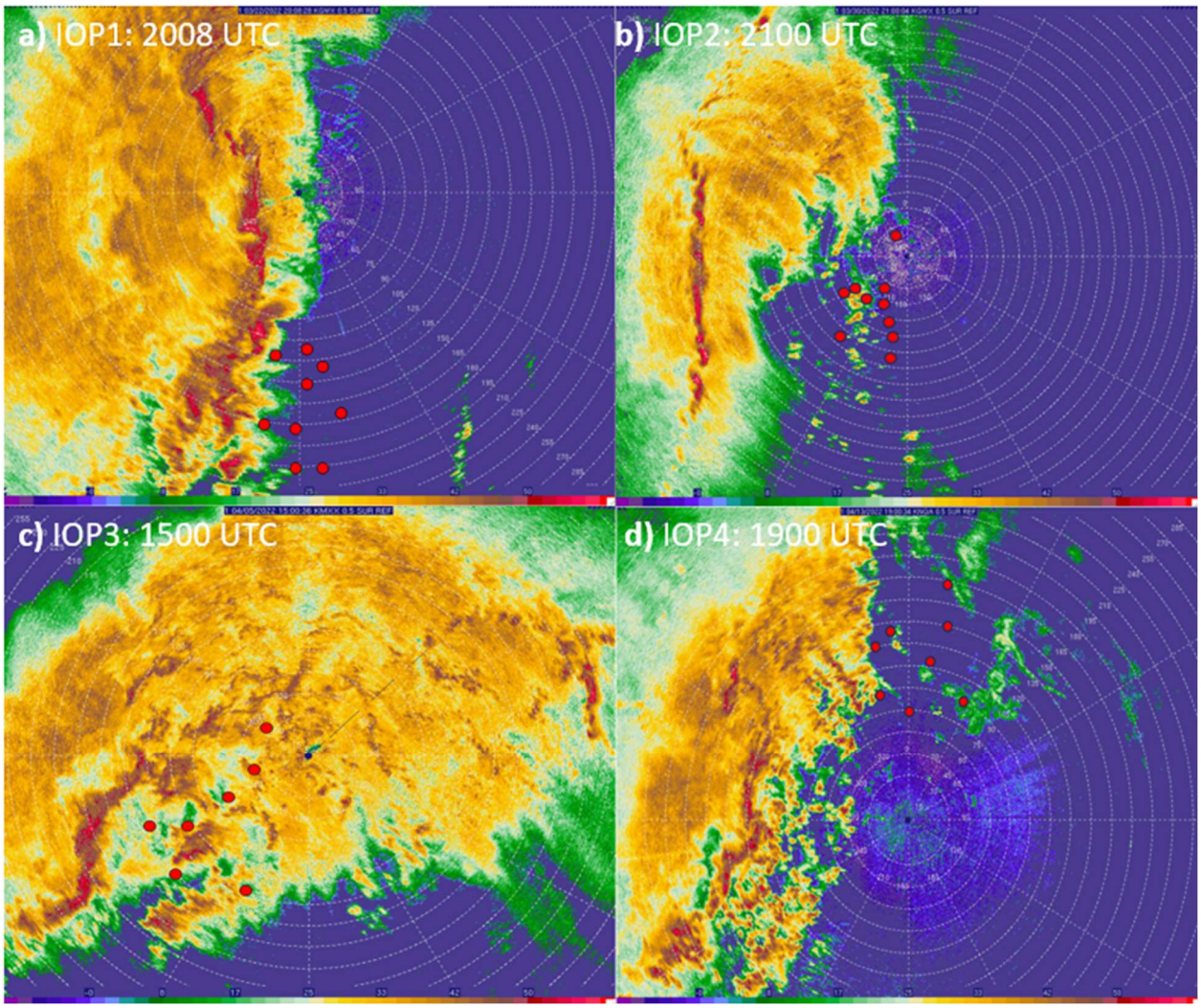

Fig. 7: The locations of soundings (red circles) launched for each IOP overlaid on 0.5˚ WSR-88D radar reflectivity (dBZ) at times given. Any sounding location seen above that is an area of precipitation was not included in the calculations for LCL and storm-relative winds. Range rings are every 25 km.

IOP	Date	Start Time (UTC)	Approx. Location
IOP-1	2022 March 22	1800	Brooksville, MS
IOP-2	2022 March 30	1900	Armory, MS
IOP-3	2022 April 5	2100	Selma, AL
IOP-4	2022 April 13	2300	Kennett, MO

Table 1: A summary of the dates, times, and locations of the PERiLS-2022 deployments. The times indicate "T_0" which was the forecasted time of the onset of deep, moist convection within the project domain. The location is based on the subdomains chosen for each IOP.

IOP	Time (UTC)	Average CAPE (J kg^{-1})	Min/Max CAPE (J kg^{-1})	0-1 km wind shear (m/s)	0-6 km wind shear (m/s)
IOP-1	18:00 – 20:00	426	3 / 1359	21.6	29.3
IOP-2	21:00 – 23:00	410	345 / 499	21.5	36.2
IOP-4	18:00 – 19:00	304	157 / 463	20.1	26.3

Table 2: A summary of the average CAPE, min/max CAPE, 0-1km average shear, and 0-6 average shear of the PERiLS 2022 deployments during the time periods of interest. IOP-3 is not listed as there was no usable environmental data from soundings.

3 Results

3.1 Z_{DR} Column Area Evolution

In the analysis of Z_{DR} column areas for all four IOPs, there was at least one time in which there was significant individual growth of a Z_{DR} column area. Once an area of interest was pinpointed in the reflectivity field, the elevation angle was chosen using the aforementioned algorithm output (e.g., bottom center panels in Fig. 6) and then the area calculated (e.g., bottom right panels in Fig. 6). As an example, from IOP1, the two times chosen show the growth of an updraft in the northern portion of the QLCS towards the end of the deployment within the PERiLS domain starting from the minimum area (Fig. 6a) to the time right before the peak value (Fig 6b). In this case, the peak value is not shown since there may have been some interference with the melting layer at the correct elevation angle. In a second example, from IOP 2, there is growth of an updraft from a southern portion of the storm as new cells from the south feed into the QLCS (Fig. 8).

Using the algorithm column area output, time series of individual updraft areas (Figs. 9a,10a,11a,12a) and total of all updraft areas within the QLCS at one time (Figs. 9b,10b,11b,12b) were constructed. Some individual updrafts, particularly in IOPs 2 and 3 (Figs. 10a and 11a) can be seen to expand or shrink on relatively short time scales (i.e., < 15 min) compared to the total area, which is consistent with previous research finding that QLCS updrafts are more transient than the deep and long-lived rotating updrafts of supercells. At some times, there is clear evidence that increases in Z_{DR} column area are correlated in time along the QLCS. For example, in IOP2 between ~21:50-22:20 UTC, there are several individual Z_{DR} columns within the QLCS that all undergo areal expansion at the same time, from areas of 0-10 km^2 to 20-80 km^2 (Fig. 10a). Later within the same IOP, from ~23:30-00:10 UTC, there are also simultaneous decreases in Z_{DR}

column area, but it is likely that there is a non-meteorological influence from the QLCS approaching the radar location and the corresponding lack of upper-level data. In IOP3 (Fig. 11a), there is not as clear a signal for correlated changes as in IOP2. The largest individual increases in Z_{DR} column area, at ~15:50, 16:15, and 17:00 UTC, all occur while other areas of the line see no appreciable changes to the areas of existing Z_{DR} column areas. The individual changes in IOP4 are a mix; initially (~19:30 UTC) there is one large increase that is not matched elsewhere, however near the end of the deployment (~20:20 UTC), two Z_{DR} columns undergo large changes at roughly the same time.

The total Z_{DR} column areas are far less noisy than the individual updrafts, as expected. Remarkably, IOP1 (Fig. 9b) has a nearly three hour long period (18:30 UTC – 19:58 UTC) in which the overall Z_{DR} column area is essentially constant with an average Z_{DR} column area of 88.5 km^2 ± 33.5 km^2. Before this time period (18:02 UTC – 18:30 UTC) the average area was 171.1 km^2 ± 61.2 km^2 and after (20:53 UTC – 22:05 UTC) the area was 158.9 km^2 ± 63.9 km^2. IOPs 2 and 4 (Figs. 10b, 12b) also have 1 hr+ time periods in which minimal changes to overall updraft area are observed. However, there are also times with large changes in overall Z_{DR} column area. Sometimes these abrupt changes are driven by one singular presumed updraft (e.g., at ~18:15 UTC in Fig. 9 and ~19:20 UTC in Fig. 12) and other times by the aforementioned correlated increases (e.g., ~22:00 UTC in Fig. 10 and ~20:20 UTC in Fig. 12).

Given the different Z_{DR} column area behaviors observed in the four IOPs, it is difficult to conclude any one dominant behavior in the evolution of Z_{DR} column area from these four cases. However, there is evidence that in some cases, there is a non-localized mechanism driving changes in updraft area proxies given the correlated changes. To investigate this idea, the following time periods were chosen based on significant individual updraft growths: IOP1- northern updraft from

21:15 to 21:45 UTC (green line in Fig. 9a); IOP2 – middle updraft 21:53 to 22:23 UTC (red line in Fig. 10a); IOP3: southern updraft 16:30 to 16:50 UTC (dark purple line in Fig. 11a); IOP4 – southern updraft 19:20 to 1935 UTC (light blue line in Fig. 12a).

. 3.2 Near-storm Environments of Expanding Z_{DR} Column Areas

Z_{DR} column areas are further investigated to see if there are links between area changes and changes in the NSE. The two environmental variables used in comparison with updraft growths are LCL height and storm-relative winds. As found by Mulholland et al. (2021) in simulated storms, higher LCL heights coincided with larger updraft sizes and work by Peters et al. (2020) found that SRH and streamwise vorticity were *not* correlated to updraft width (Fig. 2a,b), but that storm-relative winds and deep-layer shear were correlated with updraft size (Fig. 2c,d).

When the locations of each significant updraft growth were identified, only IOP2 had sounding teams collecting data in the same area where the updraft growth was taking place (Fig. 7c). IOP1 had sounding coverage in the southern portion of the domain (Fig. 7a) while the significant updraft growth at ~21:10 UTC was in the northern portion of the domain (Fig. 6a). A similar problem was found with IOP4 where the sounding coverage was in the northern part of the domain (Fig. 7d) but the updraft growth was to the south (Fig. 12a). As discussed previously, IOP3 soundings were almost all launched within significant precipitation and we cannot confidently conclude they represent the air being ingested by the QLCS. As a result, IOP2 was viewed as the best test case for such comparisons, and IOPs 1 and 4 were viewed as null cases (i.e., were there cases where the hypothesized environmental changes occurred without a corresponding change in column area?).

With this in mind, for IOP2, the sounding locations and times coincided with the growth in the Z_{DR} column area in the middle updraft (denoted in red in Fig. 6a) beginning at ~21:53 UTC. LCL heights and storm-relative winds were plotted for 21:00, 22:00, and 22:40 UTC (Fig. 13). Any soundings which had either radar or skew-T indications of precipitation contamination were not used in these plots. The overall trend of the LCL heights and surface based storm-relative winds are actually decreasing (the former more significantly) with time when the updraft area is growing, the opposite of what Peters et al. (2020) and Mulholland et al. (2021) found for supercells (Fig. 13a,b). Also, the 500 m storm-relative winds for IOP2 actually slightly increase by 22:40 UTC (Fig. 13c). For the null cases, IOPs 1 and 4 (Figs. 14, 15), the locations of the soundings did not coincide with locations of Z_{DR} column area growth, so we compare the environmental parameters to those from IOP2 to see if there were opposing trends. There is not a constant trend with both of these IOPs. For IOPs 1 and 4, LCL heights (Figs. 14a, 15a) stay almost constant with a slight average decrease. The surface and 500 m storm-relative winds (Figs. 14b,c; 15b,c) however, increase dramatically in IOP4 and less so in IOP1.

When comparing the overall magnitude of IOP2, LCL heights to IOPs 1 and 4, IOP2 has larger LCL heights (Figs. 13a, 14a, 15a). The IOP2, storm-relative winds overall are slightly stronger than in IOP4 (Figs. 13b,c; 14b,c; 15b,c), but not as noticeably in IOP1. This might indicate a more general agreement with at least Peters et al. (2020), where on smaller time scales there is not a trend present with higher LCLs and stronger updrafts. With this small sample size, it could be said that with these three QLCS's, where the LCL is generally higher and storm-relative winds are stronger, there is a greater chance of updrafts being larger along that part of the line than in other areas of the storm. However, due to the limiting domain, a more concrete correlation cannot be made between the overall larger LCL heights in IOP2 compared to that from the others. NSE

data from the northern portion of IOP2's QLCS, where there was less of a clear signal of individual updraft growths, would have to be obtained in order to compare the heights of LCLs within the ***same*** storm.

a)

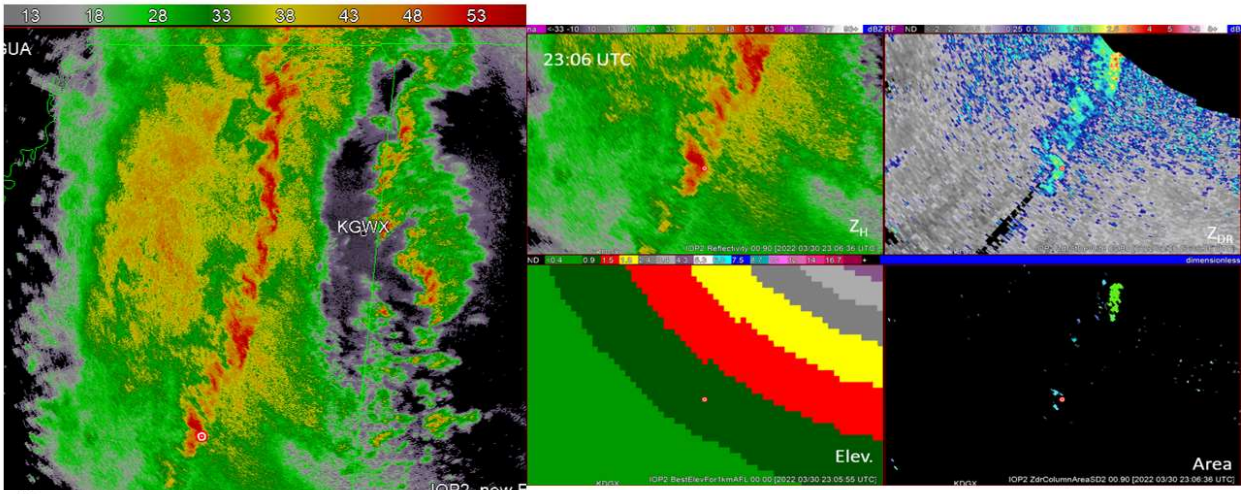

b)

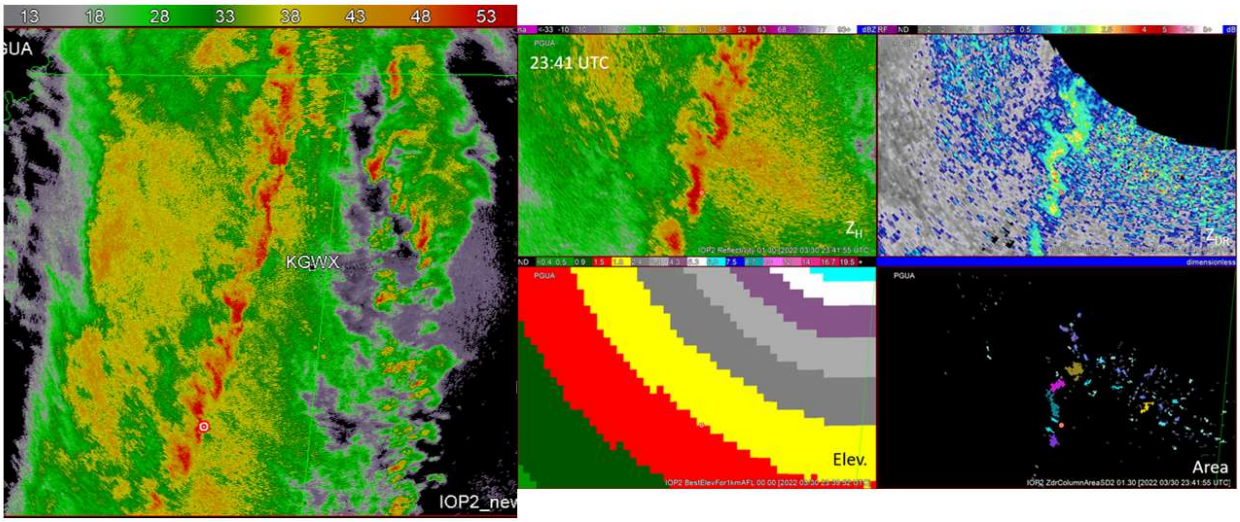

Fig. 8: Four panels depicting how Z_{DR} column area is calculated and evolving from 23:06 to 23:42 UTC in IOP2 with a snapshot of the whole QLCS at 0.5° elevation angle at each time to the left. Top left panel is reflectivity (Z_H), top right differential reflectivity (Z_{DR}), bottom left map depicting which elevation angle is closest to 1 km above 0°C level for the area of interest (indicated by red dot), and bottom right is the Z_{DR} column area. **a)** 23:06 UTC new southern updraft calculated at a 0.9° elevation angle **b)** 23:41 UTC new southern updraft calculated at 1.3° elevation angle.

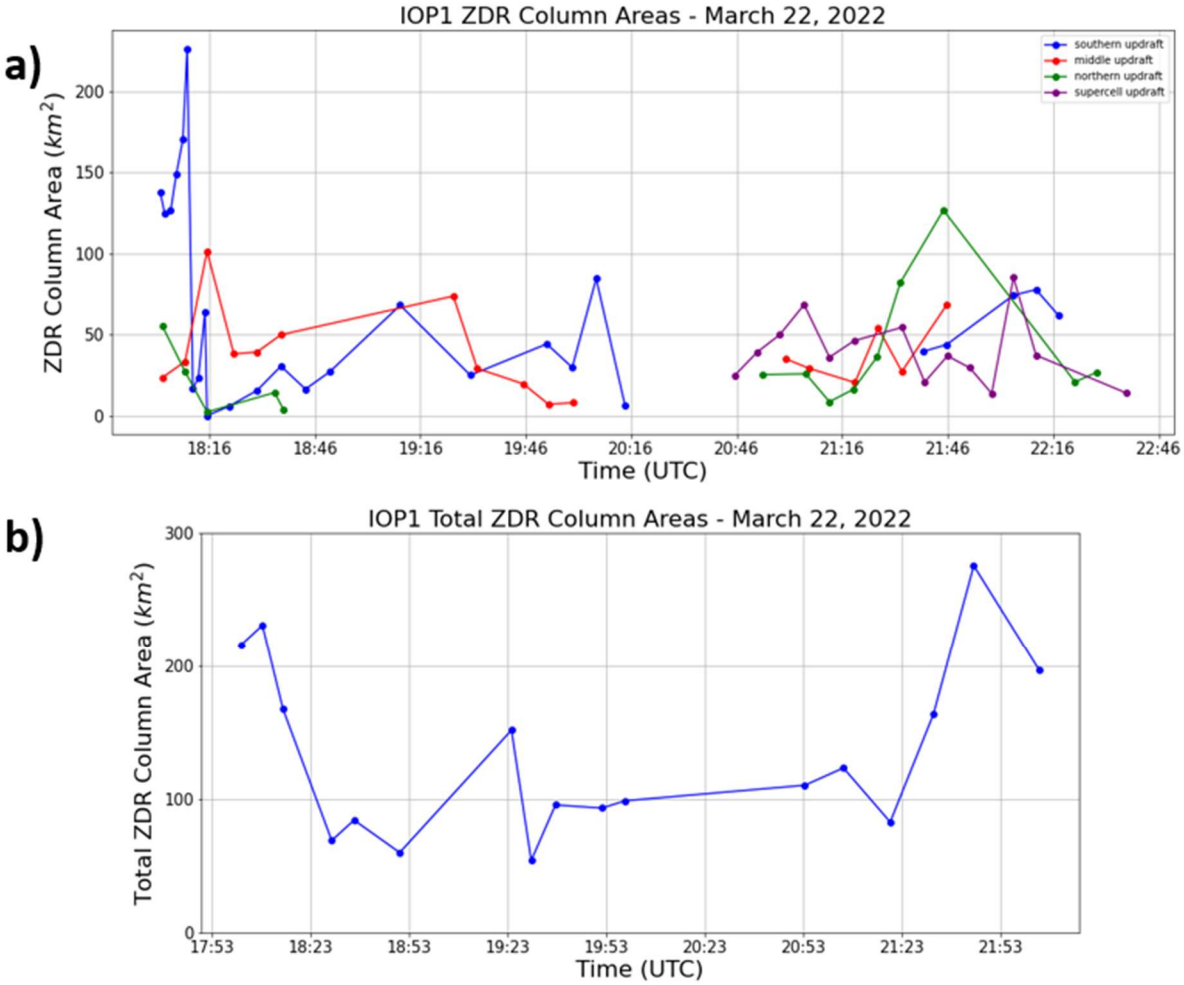

Fig. 9: IOP1 time series from 18:00-22:30 UTC: a) individual updrafts measured as Z_{DR} column areas in km^2 at radar elevation angle closest to 1 km above 0°C level and b) sum of all updrafts/areas within the QLCS at one time. The break at 20:16 UTC is from data lost as the QLCS went directly over the radar. Updrafts were re-labeled north/middle/south after this break in time.

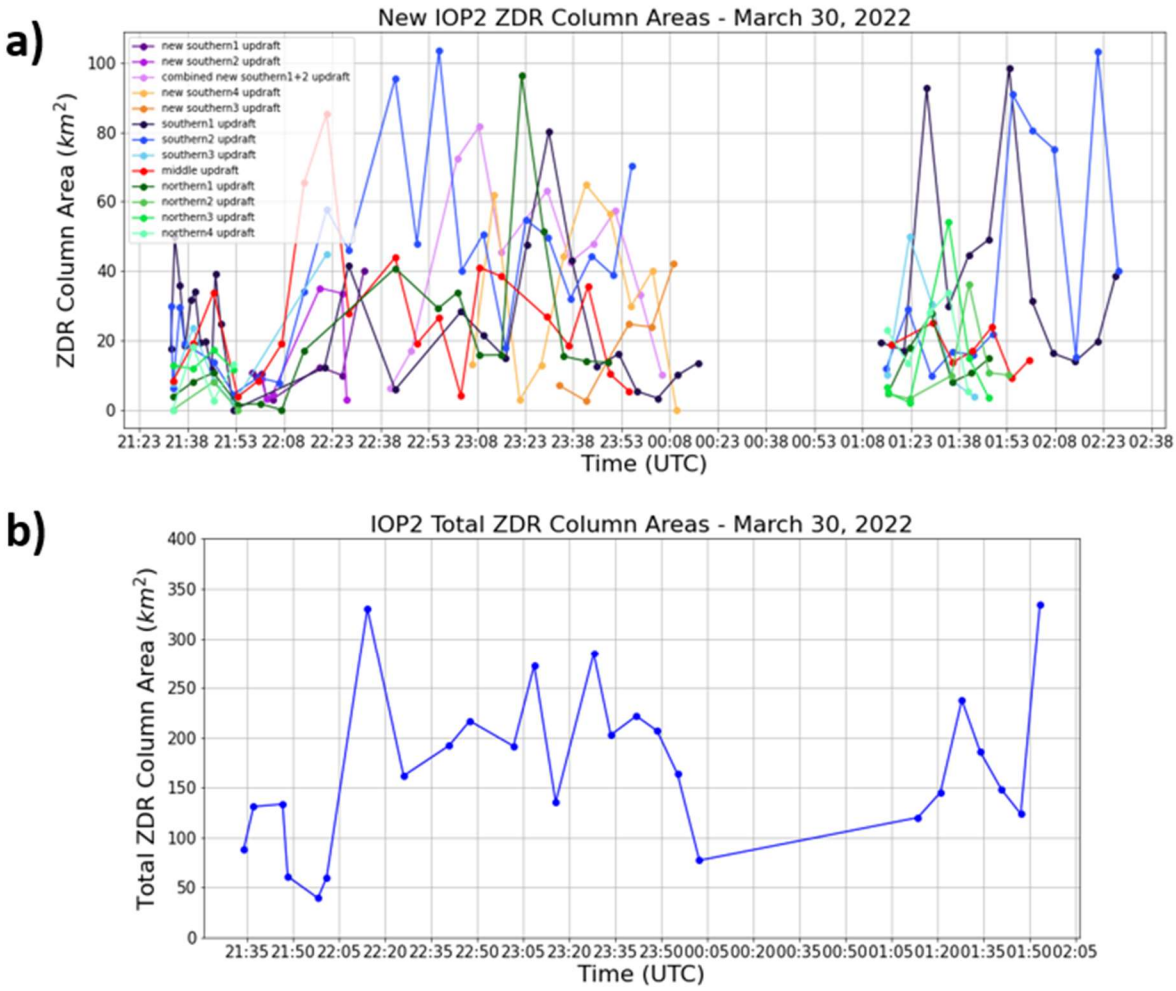

Fig. 10: IOP2 time series from 21:30-00:00 UTC: a) individual updrafts measured as Z_{DR} column areas in km^2 at radar elevation angle closest to 1 km above 0°C level and b) sum of all updrafts/areas within QLCS at one time. The break in data at 00:08 UTC is from data being lost as the QLCS went directly over the radar. Updrafts were re-labeled north/middle/south after this break in time.

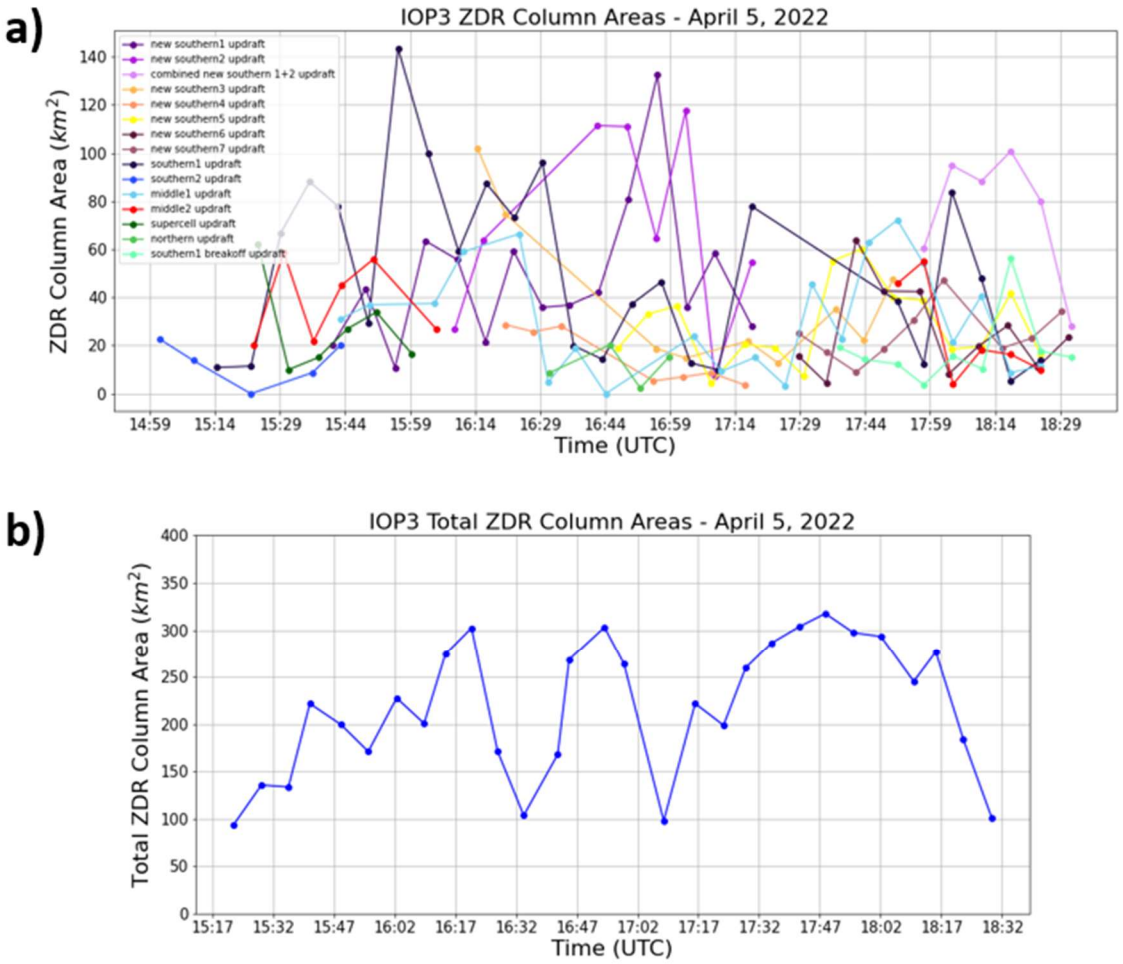

Fig. 11: IOP3 time series from 15:20 - 18:30 UTC: a) individual updrafts measured as Z_{DR} column areas in km^2 at radar elevation angle closest to 1 km above 0°C level and b) sum of all updrafts/areas within QLCS at one time.

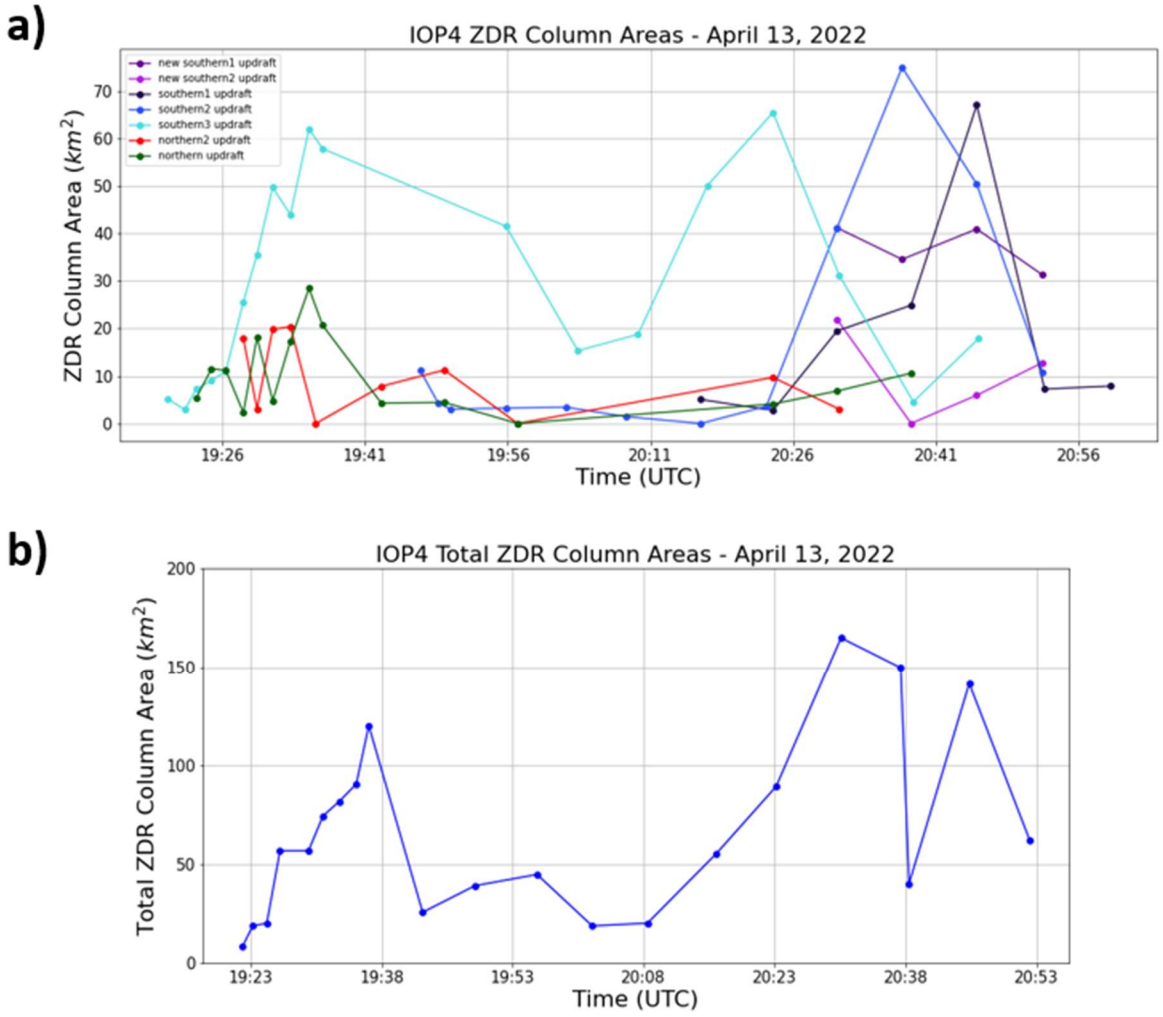

Fig. 12: IOP4 time series from 19:20-20:50 UTC: a) individual updrafts measured as Z_{DR} column areas in km^2 at radar elevation angle closest to 1 km above 0°C level and b) sum of all updrafts/areas within QLCS at one time.

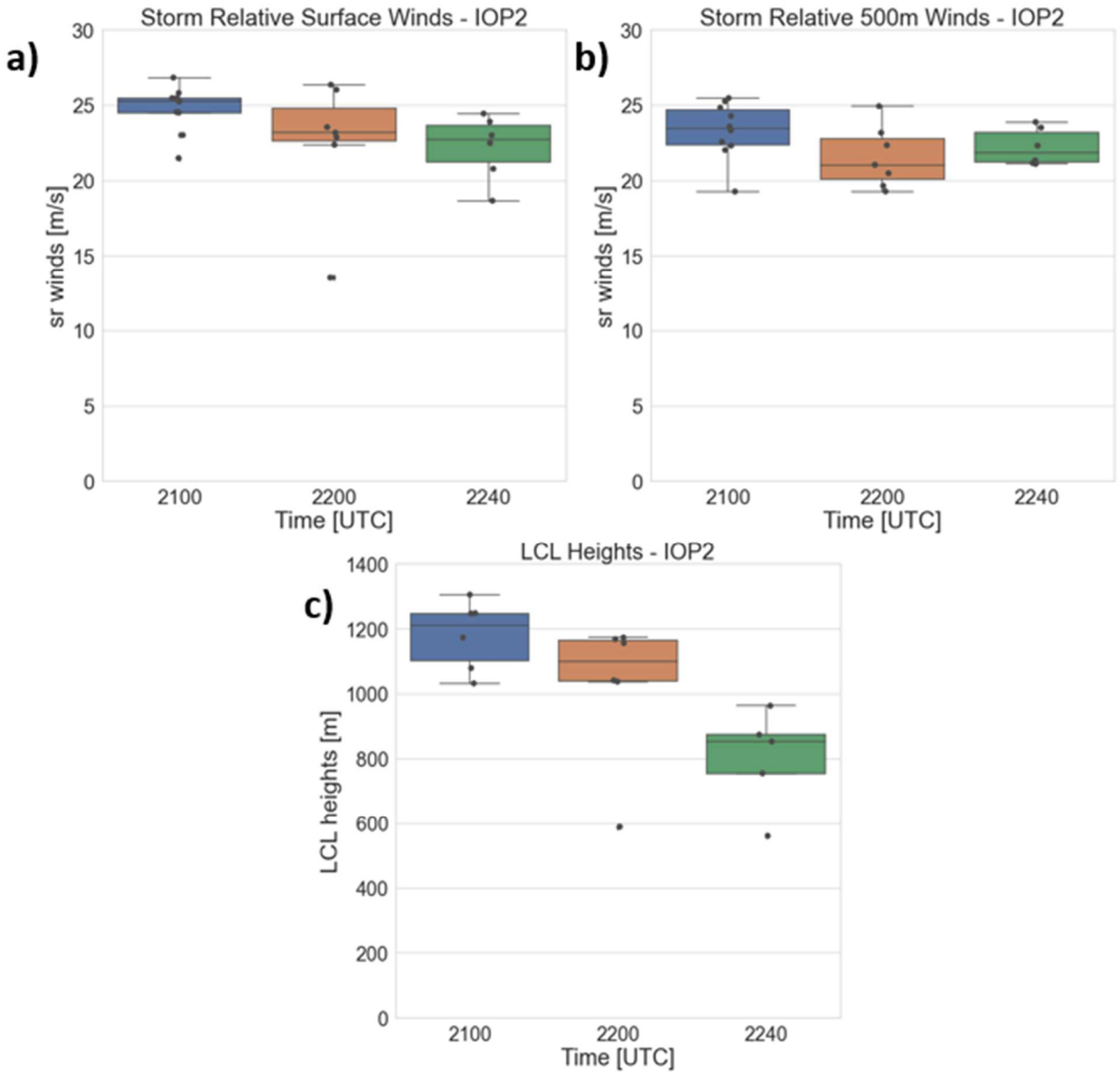

Fig. 13. Sounding data from IOP2 starting around the time when there was a significant growth in the Z_{DR} column (2000-2100 UTC) and there were soundings not launched in precipitation. a) storm-relative winds calculated from winds recorded from sounding data closest to the surface (specific heights vary) and b) storm-relative winds from recorded winds at 500m and c) LCL heights

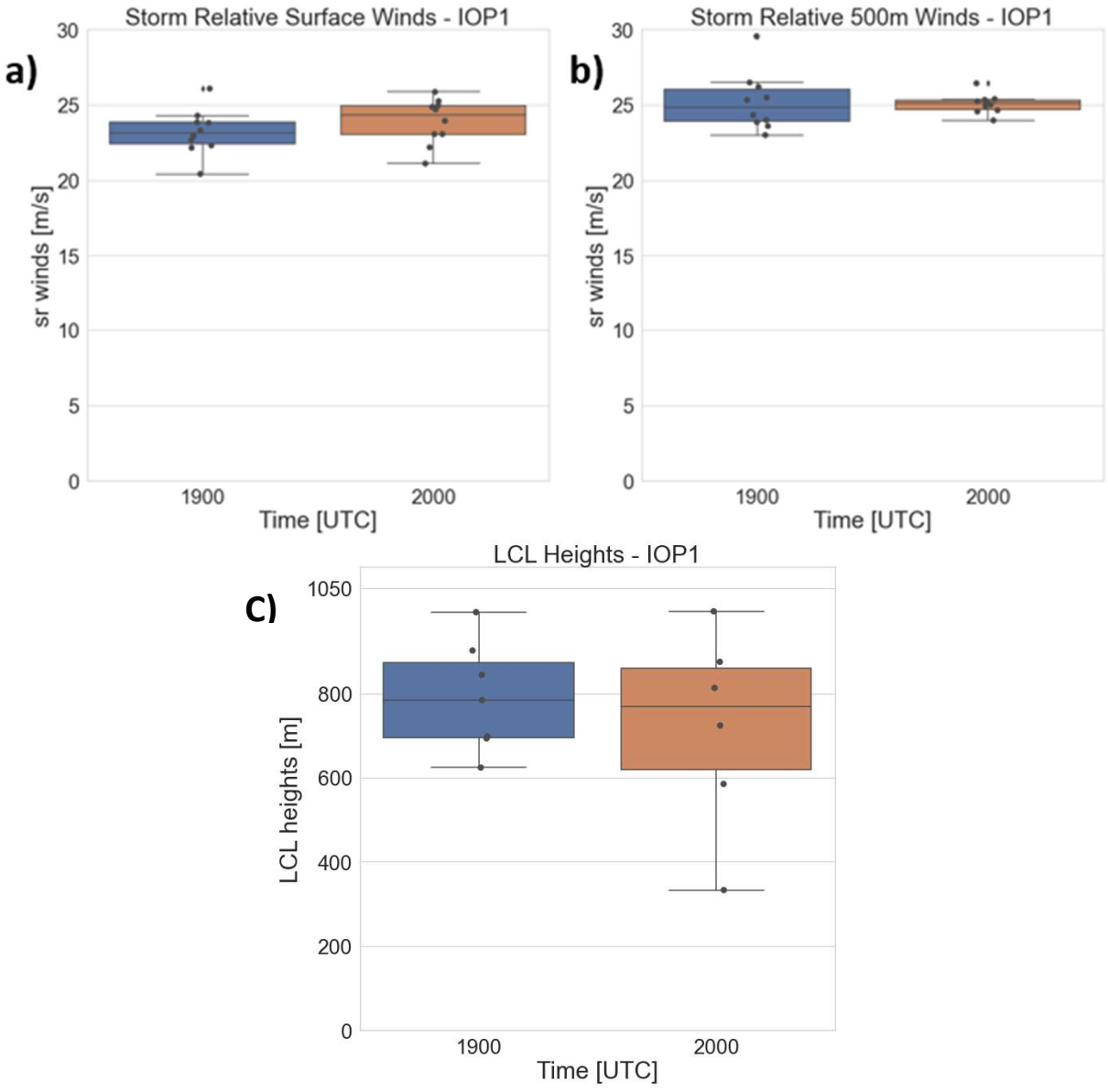

Fig. 14. Sounding data from IOP1 starting around the time when there was a significant growth in the Z_{DR} column (1900 - - 2000 UTC) and there were soundings not launched in precipitation. a) storm-relative winds calculated from winds recorded from sounding data closest to the surface (specific heights vary) and b) storm-relative winds from recorded winds at 500m and c) LCL heights

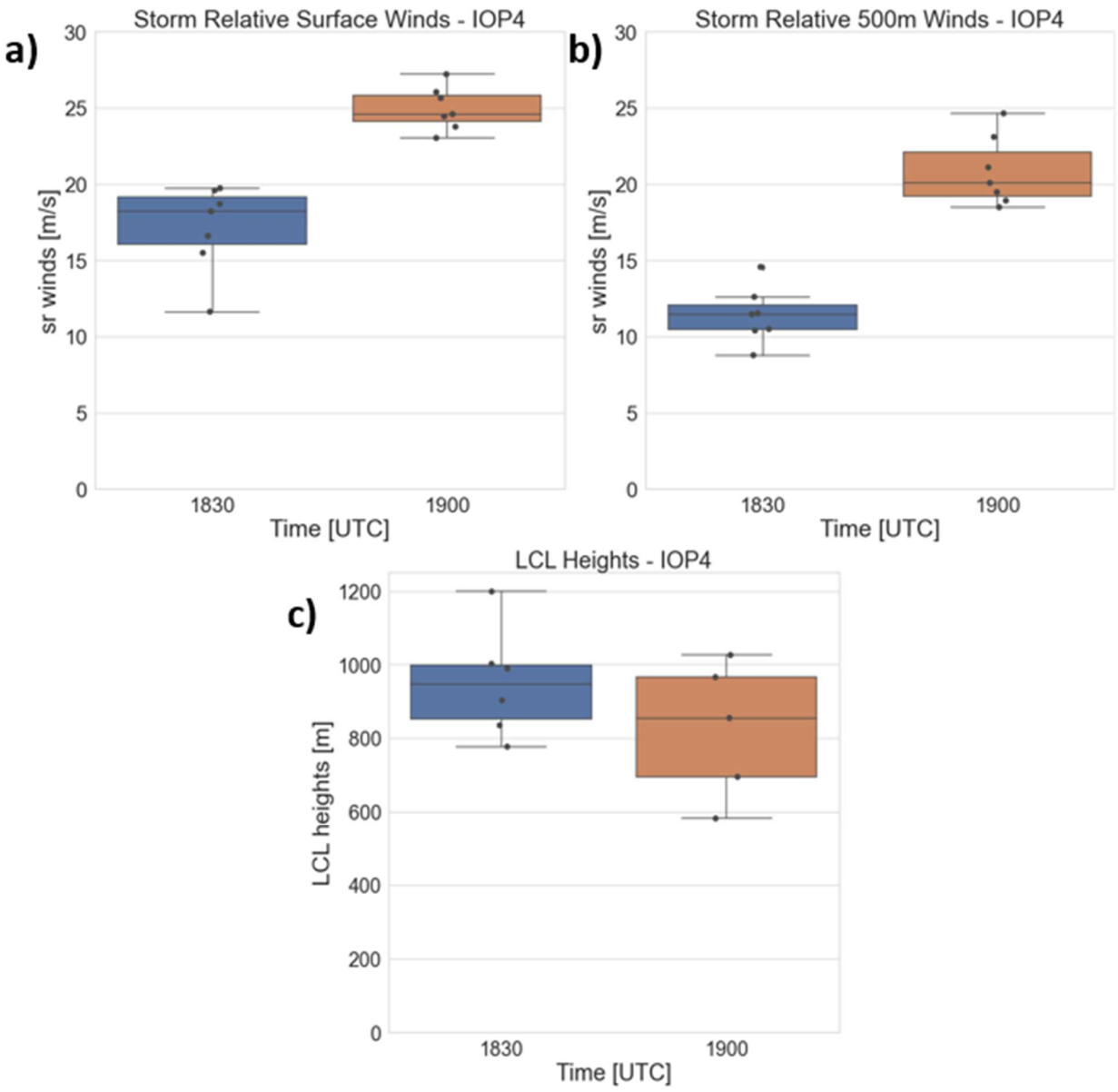

Fig. 15. Sounding data from IOP4 starting around the time when there was a significant growth in the Z_{DR} column (1830-1900 UTC) and there were soundings not launched in precipitation. a) storm-relative winds calculated from winds recorded from sounding data closest to the surface (specific heights vary) and b) storm-relative winds from recorded winds at 500m and c) LCL heights

4 Discussion

The Z_{DR} column areas in the QLCSs varied in having long periods of time with near-constant total area and also times where there are large abrupt increases in area. The latter increasing periods typically were driven by one or two storm cell / updraft cores within the larger line. The most interesting aspect of the time evolution is the correlated increases where multiple parts of the line would undergo increases in updraft area at roughly the same time. What do the correlated increases indicate? Our view is that it is most likely that the along-line near-storm environment the QLCS encounters becomes more favorable for greater mass flux and updraft area. In other words, it is reasonable that the line would encounter similar environmental changes at roughly the same time. Less likely in our view is that something internal to the QLCS drives the correlated increases as whatever complex process would be contributing to the increase in vertical mass flux (e.g., enhanced descending rear-inflow jet) would have to occur at the same time within several individual cells. That cannot be ruled out, but we believe the most likely reason for the correlated increases is the simplest one: the QLCS moves into a more favorable environment for larger updrafts. Also, the low number of IOPs (climatology informed an estimate of 7 PERiLS IOPs per year) also meant far too few tornado cases within the domain for a direct comparison between area proxy and tornado intensity.

On that topic, the main results of the comparative analysis indicate a clear null result. There is not sufficient evidence that an increase in storm-relative winds and/or LCL height increased in coordination with the increase in Z_{DR} column area. There are several possibilities for this result. First is the reality that the field project data are not as favorable for this analysis as we would have hoped. Despite being a large field project, the PERiLS domain was still a small subset of the QLCS domains and therefore often did not line up with where we found the most interesting

column area evolution. In addition, three of the four IOPs contained significant precipitation forward of the main convective line which affected some of the soundings ability to accurately capture the storm environment. The end result is that the sample size of sounding-area comparisons completed in this study is not sufficient to rule out that there is a relationship between storm-relative winds, LCL heights, and updraft area proxies. There were also many areas for potential error within this study, despite our best effort to limit errors and mitigate subjectivity, which could have contributed to the null result. The main error culprit is the messy and subjective nature of compiling the Z_{DR} column areas and choosing the correct level at which to record the column area. Computing the storm motion also left room for possible error as the leading edge of the storm was estimated by hand based on radar data, which is unavoidably looking at different heights in the storm depending on the distance from the radar.

Another possibility is that the dynamics of QLCSs are different enough from supercells that the environmental drivers of large updrafts are different. Most of the theoretical framework for larger updrafts and environmental controls on updrafts is focused on supercells, and our attempt to superimpose those results on QLCSs without consideration of the different processes the systems undergo also likely contribute to the null result. Indeed, as previously discussed, the results of Marion et a. (2019) and Sessa and Trapp (2020) indicate the signal between tornado intensity and updraft area proxy is weaker in QLCSs compared to supercells. As a result, it stands to reason that there are other or different factors at play with QLCSs.

5 Summary and Future Work

5.1 Summary

The main focus of this study is the spatial and temporal changes of updraft size within QLCSs using Z_{DR} column areas as a proxy for updraft area. The PERiLS 2022 field campaign, which consisted of four IOPs (Table 1) of data from QLCSs using various instrumentation such as mobile radars, sounding and profiling systems, mobile mesonets, disdrometers, and lightning mapping arrays, provided an opportunity to compare updraft area to the storm environment. WSR-88D radar data was used in this study to identify Z_{DR} columns and estimate their area to approximate the size of the updraft. Radiosonde data from a number of different PERiLS teams were used in the NSE data analysis as they provided unique environmental data as close to the storm as possible at more frequent time increments than traditional soundings.

In each IOP, there was at least one significant individual updraft growth which grew and dissipated on shorter timescales than the lifetime of the QLCS: IOP1- northern updraft from 21:15 to 21:45 UTC (Fig. 9a); IOP2 – middle updraft 21:53 to 22:23 UTC (Fig. 10a); IOP3: southern updraft 16:30 to 16:50 UTC (Fig. 11a) ; IOP4 – southern updraft 19:20 to 1935 UTC (Fig. 12a). This is consistent with the idea that QLCS updrafts are weaker and more transient in nature than in supercells (Sessa and Trapp 2020). The periods listed above became the times and locations of focus for each IOP. IOP3 was not used in the analysis for the NSE since by the time the QLCS had formed into a discernable line, the soundings were all launched in precipitation (Fig. 7). The location of soundings for IOPs 1 and 4 did not coincide with the location of significant updraft growth so those were used as "null" cases to compare to IOP2 where the soundings were lined up with the area of updraft growth.

The LCL heights and storm-relative (surface and 500m) winds were plotted for IOPs 1, 2 and 4 around the time of each updraft growth. Contrary to the findings of Peters et al. (2020) and Mulholland et al. (2021), the LCL heights and storm-relative winds in IOP2 generally decreased as updraft growths increased (Fig. 13). In the null cases (IOPs 1 and 4), when updraft growth was stagnant or not significant, there was an increase or no change in LCL heights and storm-relative winds (Figs. 14 and 15). A note of agreement with Peters et al. (2020) could be said for the overall LCL heights; IOP2 has overall larger heights than in IOPs 1 and 4.

5.2 Future Work

Despite inconclusive results, there is an opportunity to expand this project or change the focus. One possibility is to continue to study what is the primary driver of the growths of updrafts within QLCSs. The idea of larger LCL heights and storm-relative winds leading to larger updrafts cannot be completely ruled out due to the small sample size. Data obtained in PERiLS-2023 should be widely available in the coming months so another five IOPs could be added to the dataset. A larger dataset would also provide comparisons between similar QLCS modes (horizontal vs vertical orientation, pre-convective vs trailing precipitation, and symmetrical vs asymmetrical) and if there is any consistency in updraft growth or NSE controls. Since the ZDR column area detection algorithm is programmed to only run WSR-88D data, other avenues to automate the area using the mobile radars from PERiLs could also provide additional radar coverage. With a lot of NSE data having to be discarded due to precipitation contamination, comparisons with PERiLs data to the RAP or model data might fill in any gaps or can justify the validity of PERiLs data.

Another possibility is to alter the focus. For example, very recent studies have implicated updraft size as a potential important contributor to large hail formation (e.g., Homeyer et al. 2023)

and mesovortex formation. The nine total IOPs could be mined for radar- and/or report-based hail and use specialized runs of Multi-Radar Multi-Sensor (MRMS) azimuthal shear tracks (as a proxy for mesovortices) to compare with individual updraft core sizes. To what extent are ZDR columns present when a mesovortex or large hail occurs and is there a relationship between column area and hail size or mesovortex intensity? Another possibility is to incorporate data from the lightning mapping arrays to determine to what extent individual and total updraft size is related to electrification in QLCSs. As more work is completed in studying updraft areas, new or additional environmental variables may be implicated as drivers. For example, work published earlier this year in Peters et al. (2023) formulated a new version of CAPE incorporating entrainment (ECAPE), which should better connect instability to updraft area and mass flux. We anticipate that additional work will better elucidate the many open questions regarding updraft sizes in QLCSs.

References

Ashley, W. S., A. M. Haberlie, J. Strohm, 2019: A Climatology of Quasi-Linear Convective Systems and Their Hazards in the United States. *Wea. Forecasting*, **34**, 1605-1631, https://doi.org/10.1175/WAF-D-19-0014.1

Ashley, W. S., A. J. Krmenec, and R. Schwantes, 2008: Vulnerability Due to Nocturnal Tornadoes. *Wea. Forecasting*, **23**, 795-807, https://doi.org/10.1175/2008WAF2222132.1.

Bedka, K., Brunner J., R. Dworak, W. Feltz, J. Otkin, and T. Greenwald, 2010: Objective Satellite-based Detection of Overshooting Tops Using Infrared Window Channel Brightness Temperature Gradients. *J. Appl. Meteor. Climatol.,* **49**, 181-201, https://doi.org/10.1175/2009JAMC2286.1

Brotzge, J., S. Nelson, R. L. Thompson, and B. T. Smith, 2013: Tornado Probability of Detection and Lead Time as a Function of Convective Mode and Environmental Parameters. *Wea. Forecasting*, **28**, 1261-1276, https://doi.org/10.1175/WAF-D-12-00119.1.

Coffer, B.E. and P.M. Markowski, 2018: Comments on The Regulation of Tornado Intensity by Updraft Width. *J. Atmos. Sci*., **75**, 4049-4056, https://doi.org/10.1175/JAS-D-18-0170.1.

Coffer, B.E., M.D. Parker, R.L. Thompson, B.T. Smith, R.E. Jewell, 2019: Using Near-Ground Storm Relative Helicity in Supercell Tornado Forecasting. *Wea. Forecasting*, **34**, 1417-1435, https://doi.org/10.1175/WAF-D-19-0115.1.

Coniglio, M. C., S. F. Corfidi, J. S. Kain, 2012: Views on Applying RKW Theory: An Illustration Using the 8 May 2009 Derecho-Producing Convective System. *Mont. Weather Rev.,* **140**, 1023-1043, https://doi.org/10.1175/MWR-D-11-00026.1

French, M. M. and D. M. Kingfield, 2021: Tornado Formation and Intensity Prediction Using Polarimetric Radar Estimates of Updraft Area. *Wea. Forecasting*, **36**, 2211-2231, https://doi.org/10.1175/WAF-D-21-0087.1

Fritsch, J. M., J. D. Murphy, J. S. Kain, 1994: Warm Core Vortex Amplification over Land. *J. Atmos. Sci.,* **51**, 1780-1807, https://doi.org/10.1175/1520-0469(1994)051<1780:WCVAOL>2.0.CO;2

Haberlie, A. M. and W.S Ashley, 2018: A Method for Identifying Midlatitude Mesoscale Convective Systems in Radar Mosaics. Part I: Segmentation and Classification. *J. Appl. Meteorol. Climatol*, **57**, 1575-1598, https://doi.org/10.1175/JAMC-D-17-0293.1

Homeyer, C. R., E. M. Murillo, and M. R. Kumjian, 2023: Relationships between 10 Years of Radar-Observed Supercell Characteristics and Hail Potential. *Mon. Wea. Rev.*, **151**, 2609–2632, https://doi.org/10.1175/MWR-D-23-0019.1.

Houze, R. A., Jr., S. A. Rutledge, M. I. Biggerstaff, B. F. Smull, 1989: Interpretation of Doppler Weather Radar Displays of Midlatitude Mesoscale Convective Systems, *Bull. Am. Meteorol. Soc*., **70**, 608-619, https://doi.org/10.1175/1520-0477(1989)070<0608:IODWRD>2.0.CO;2

Houze, R. A., Jr. 2018: 100 Years of Research on Mesoscale Convective Systems. *Meteorol. Monogr.,* **59**, 17.1-17.54, https://doi.org/10.1175/AMSMONOGRAPHS-D-18-0001.1

Kain, J. S., S. J. Weiss, D. R. Bright, M. E. Baldwin, J. J. Levit, G. W. Carbin, C. S. Schwartz, M. L. Weisman, K. K. Droegemeier, D. B. Weber, K. W. Thomas, 2008: Some Practical Considerations Regarding Horizontal Resolution in the First Generation of Operational Convection-Allowing NWP. *Wea. Forecasting*, **23**, 931-952, https://doi.org/10.1175/WAF2007106.1

Kingfield, D. M. and J. C. Picca, 2018: Development of an Operational Convective Nowcasting Algorithm Using Raindrop Size Sorting Information from Polarimetric Radar Data. *Wea. Forecasting,* **33**, 1477-1495, https://doi.org/10.1175/WAF-D-18-0025.1

Kumjian, M. R and A. V. Ryzhkov, 2008a: Polarimetric Signatures in Supercell Thunderstorms. *J. Appl. Meteor. Climatol*., **47**, 1940-1961, https://doi.org/10.1175/2007JAMC1874.1

Kumjian, M. R., A. P. Khain, N. Benmoshe, E. Ilotoviz, A.V. Ryzhkov, V.T.J Phillips, 2014: The Anatomy and Physics of Z_{DR} Columns: Investigating a Polarimetric Radar Signature with a Spectral Bin Microphysical Model. *J.Appl. Meteor. Climatol*., **53**, 1820-1843, https://doi.org/10.1175/JAMC-D-13-0354.1

Kuster, C. M., J. C. Snyder, T. J. Schuur, T. T. Lindley, P. L. Heinselman, J. C. Furtado, J. W. Brogden, and R. Toomey, 2019: Rapid-Update Radar Observations of Z_{DR} Column Depth and Its Use in the Warning Decision Process. *Wea. Forecasting*, **34**, 1173-1188, https://doi.org/10.1175/WAF-D-19-0024.1

Marion, G. R., R. J. Trapp, S. W. Nesbitt, 2019: Using Overshooting Top Area to Discriminate Potential for Large, Intense Tornadoes. *Geophysical Research Letters*, **46**, 12520-12526. https://doi.org/10.1029/2019GL084099

Marion, G. R and R. J. Trapp, 2021: Controls of Quasi-Linear Convective System Tornado Intensity. *J. Atmos. Sci.,* **78**, 1189-1205, https://doi.org/10.1175/JAS-D-20-0164.1

Mulholland, J. P., J. M. Peters, and H. Morrison, 2021: How Does LCL Height Influence Deep Convective Updraft Width? *Geophys. Res.*, **48**, e2021GL093316, https://doi.org/10.1029/2021GL093316

Peters, J. M., C. J. Nowotarski, J. P. Mulholland, and R. L. Thompson, 2020: The Influences of Effective Inflow Layer Streamwise Vorticity and Storm-relative Flow on Supercell Updraft Properties. *J. Atmos. Sci.,* **77**, 3033-3057, https://doi.org/10.1175/JAS-D-19-0355.1

Peters, J. M., D. R. Chavas, C. Su, H. Morrison, and B. E. Coffer, 2023: An Analytic Formula for Entraining CAPE in Midlatitude Storm Environments. *J. Atmos. Sci.*, **80**, 2165–2186, https://doi.org/10.1175/JAS-D-23-0003.1.

Picca, J. C., M. R. Kumjian, and A. V. Ryzhkov, 2010: Z_{DR} Columns as a Predictive Tool for Hail Growth and Storm Evolution. Preprints, The 25th Conf. on Severe Local Storms, Denver, CO, *Amer. Meteor. Soc*., **11.3**. URL https://ams.confex.com/ams/25SLS/techprogram/paper_175750.htm

Schumacher, R. S and K. L. Rasmussen, 2020: The Formation, Character and Changing Nature of Mesoscale Convective Systems. *Nat. Rev. Earth Environ.,* **1**, 300-314, https://doi.org/10.1038/s43017-020-0057-7

Schwartz, C. S., J. S. Kain, S. J. Weiss, M. Xue, D. R. Bright, F. Kong, K. W. Thomas, J. J. Levit, M. C. Coniglio, 2009: Next-Day Convection-Allowing WRF Model Guidance: A Second Look at 2-km versus 4-km Grid Spacing. *Mont. Weather Rev*., **137**, 3351-3372, https://doi.org/10.1175/2009MWR2924.1

Sessa, M. F and R. J. Trapp, 2020: Observed Relationship between Tornado Intensity and Pretornadic Mesocyclone Characteristics. *Wea. Forecasting*, **35**, 1243-1261, https://doi.org/10.1175/WAF-D-19-0099.1

Smith, B. T., R. L. Thompson, J. S. Grams, C. Broyles, and H. E. Brooks, 2012: Convective Modes for Significant Severe Thunderstorms in the Contiguous United States. Part I: Storm Classification and Climatology. *Wea. Forecasting*, **27**, 1114-1135, https://doi.org/10.1175/WAF-D-11-00115.1.

Snyder, J. C., A. V. Ryzhkov, M. R. Kumjian, A. P. Khain, and J. Picca, 2015: A Z_{DR} Column Detection Algorithm to Examine Convective Storm Updrafts. *Wea. Forecasting*, **30**, 1819–1844, https://doi.org/10.1175/WAF-D-15-0068.1.

Snyder, J. C., H. B. Bluestein, D. T. Dawson II, Y. Jung, 2017: Simulations of Polarimetric, X-Band Radar Signatures in Supercells. Part II: ZDR Columns and Rings and KDP Columns, *J. Appl. Meteor. Climatol*., **56**, 2001-2026, https://doi.org/10.1175/JAMC-D-16-0139.1

Stensrud, D. J., M. C. Coniglio, R. P. Davies-Jones, J. S. Evans, 2005: Comments on "'A Theory for Strong Long-Lived Squall Lines' Revisited". *J. Atmos. Sci.,* **62**, 2989-2996, https://doi.org/10.1175/JAS3514.1

Trapp, R. J., G. R. Marion, and S. W. Nesbitt, 2017: The Regulation of Tornado Intensity by Updraft Width. *J. Atmos. Sci*., **74**, 4199-4211, https://doi.org/10.1175/JAS-D-16-0331.1

Tuftedal, K. S., M. M. French, D. M. Kingfield, and J. C. Snyder, 2021: Observed Bulk Hook Echo Drop Size Distribution Evolution in Supercell Tornadogenesis and Tornadogenesis Failure. *Mon. Wea. Rev.*, **149**, 2539–2557, https://doi.org/10.1175/MWR-D-20-0353.1.

Warren, R. A., H. Richter, H. A. Ramsay, S. T. Siems, and M. J. Manton, 2017: Impact of Variations in Upper-level Shear on Simulated Supercells. *Mon. Wea. Rev.,* **145**, 2659-2681, https://doi.org/10.1175/MWR-D-16-0412.1

Wheatley, D. M., and R. J. Trapp, 2008: The effect of mesoscale heterogeneity on the genesis and structure of mesovortices within quasi-linear convective systems. *Mon. Wea. Rev*., **136**, 4220–4241, https://doi.org/10.1175/2008MWR2294.1.

Yang, Q., R. A. Houze, L. R. Leung, Z. Feng, 2017: Environments of Long-lived Mesoscale Convective Systems Over the Central United States in Convection Permitting Climate Simulations. *J. Geophys. Res.,* **122**, 13,288-13,307, https://doi.org/10.1002/2017JD027033